MANAGEMENT OF CRYOGENIC PROPELLANTS IN A FULL-SCALE ORBITING SPACE VEHICLE

by Raymond F. Lacovic, Frederick C. Yeh,
Steven V. Szabo, Jr., R. J. Brun,
Andrew J. Stofan, and James A. Berns

Lewis Research Center
Cleveland, Ohio

MANAGEMENT OF CRYOGENIC PROPELLANTS IN A FULL-SCALE

ORBITING SPACE VEHICLE

By Raymond F. Lacovic, Frederick C. Yeh, Steven V. Szabo, Jr.,
R. J. Brun, Andrew J. Stofan, and James A. Berns

Lewis Research Center
Cleveland, Ohio

NATIONAL AERONAUTICS AND SPACE ADMINISTRATION

CONTENTS

MANAGEMENT OF CRYOGENIC PROPELLANTS IN A FULL-SCALE
ORBITING SPACE VEHICLE

by Raymond F. Lacovic, Frederick C. Yeh, Steven V. Szabo. Jr..
R. J. Brun, Andrew J. Stofan, and James A. Berns

Lewis Research Center

SUMMARY

Some lunar and deep space missions require a space vehicle that can restart its engines after a coast period in space. An orbiting space vehicle using cryogenic propellants requires that the propellants be positioned in the tank to ensure gaseous venting and liquid feed to the engine for restart.

The fourth and eighth Atlas-Centaur vehicles (AC-4 and AC-8) were launched to study cryogenic propellant management during coast. The AC-4 flight showed that propellant management cannot be defined solely by the Bond number (ratio of acceleration to surface tension forces). Energies imparted to the propellants at engine cutoff, during coast, and at engine restart must be considered. On the AC-4 flight, kinetic energies imparted to the liquid hydrogen at first engine cutoff caused liquid motion within the hydrogen tank resulting in subsequent venting of liquid hydrogen rather than gaseous hydrogen. The vented liquid impinged on the vehicle causing it eventually to tumble out of control. The AC-8 vehicle was modified to reduce and/or control the energies transmitted to the propellant. Energy dissipators were installed on the hydrogen tank pressurization line and boost pump return flow lines. A balanced thrust hydrogen vent system was installed to reduce vehicle disturbances. A slosh baffle was installed in the hydrogen tank and a thrust schedule (with thrust levels increased over AC-4) for propellant settling and retention was established. These modifications reduced the total kinetic energy at first engine cutoff from 200 foot-pounds (270 J) on AC-4 to less than 50 foot-pounds (68 J) on AC-8. An additional 8400 foot-pounds (1140 J) of energy theoretically could have been transmitted to the liquid hydrogen on AC-4 during the coast and engine restart periods if the mission had been successful. This was reduced to approximately 20 foot-pounds (27 J) on AC-8.

In addition to verifying propellant management, the AC-8 flight provided data on the thermal environment of the hydrogen tank during the coast period. The information obtained on heat inputs to the tank was used to establish the capability of the hydrogen vent system. Also, a thermal survey was made of the hydrogen tank ullage; this survey provided information on temperature stratification of the ullage gas. The flight of AC-8 demonstrated a practical method for control of a cryogenic propellant in a full-scale orbiting space vehicle. The method of propellant control established for the Centaur vehicle is applicable to any space vehicle having short-term storage of cryogenic propellants in space.

INTRODUCTION

In 1958 the United States initiated the Centaur project as a high-energy liquid propellant launch vehicle for space missions. The vehicle was conceived as consisting of a modified Atlas ICBM and a Centaur second stage. Its intended use was for high-altitude satellites, space probes to the Moon and to Venus and Mars, and other deep space flights. To maximize the payload capability of the vehicle, the high-energy combination of liquid hydrogen as the fuel and liquid oxygen as the oxidizer were selected. The prime mission of the Atlas-Centaur vehicle was to launch the Surveyor spacecraft. Other missions being planned include unmanned exploration of the planets in the solar system. The general configuration of an Atlas-Centaur vehicle, including a mass model of the Surveyor spacecraft is shown in figure 1.

For lunar as well as other missions the need often arises for a vehicle to possess a "two-burn" capability, that is, the engines should be able to restart after a coasting period in space. In the case of the lunar mission, the lighting conditions on the Moon limit the available launch opportunities for a direct ascent to only certain months of the year. The launch opportunities can be extended by the use of a two-burn parking orbit ascent in which the vehicle is first inserted into a predetermined orbit around the Earth, before being placed in the trajectory for lunar intercept. A Surveyor two-burn flight plan involving a coasting period is shown in figure 2.

During the coasting period, the propellants in the tank are essentially in a weightless state (zero gravity) unless external forces, such as drag, are acting on the vehicle. For cryogenic propellants, weightlessness creates a unique problem in propellant management. The absorption of thermal energy causes the cryogens to evaporate, which results in an increase in the tank pressures. The boiloff gas must be vented periodically in order to maintain the tank pressure within allowable structural limits. If the propellant is scattered randomly throughout the tank or is located at the vent exit, tank venting may release liquid along with the boiloff gases. Also, a scheduled engine restart is not certain unless liquid is retained at the engine inlet.

Many methods of propellant retention and control have been considered in the literature (refs. 1 to 3), such as, capillary systems, which utilize surface tension to retain and position propellants; positive expulsion devices (bladders and diaphragms); supercritical storage (no defined liquid-vapor interface); thixotropic propellants in which the addition of colloidal solid particles causes the propellants to form a gel; dielectrophoresis, which utilizes a nonuniform electric field to separate liquid and vapor; and inertial systems, which provides acceleration fields for liquid-vapor separation. With the exception of the inertial system, all the methods mentioned previously have serious drawbacks at their current state of development for propellant retention and control on a

vehicle such as the Centaur.

The purpose of this report is to define the problems of propellant management that are encountered in a full-scale vehicle, and to present concepts and practical methods for their solution as demonstrated by the flights of the Atlas-Centaur AC-4 and AC-8 vehicles. The vehicles were launched by General Dynamics/Convair under the direction of the Lewis Research Center for the purpose of demonstrating launch vehicle capability and of studying propellant management during the coasting period. The concepts and methods used for propellant management and the results of the flights are discussed herein.

SYMBOLS

A   area, ft^2 (m^2)

a   acceleration, ft/sec^2 (m/sec^2)

D   diameter, ft (m)

g a/g_c

g_c gravitational acceleration at Earth's surface, 32.174 ft/sec^2 (9.8 m/sec^2)

H   height, ft (m)

h   enthalpy, Btu/lb_m (J/kg)

M   mass, lb_m (kg)

$\dot{M}$ mass flow rate, $\text{lb}_m\text{/sec}$ (kg/sec)

$\mathcal{M}$ magnification factor

P   pump power, hp (W)

Q   thermal energy, Btu (J)

q   heat flux, $\text{Btu/(hr)(ft}^2)$; (W/m^2)

r   radius, ft (m)

t   time, sec

U   internal energy, Btu/lb_m (J/kg)

V   velocity, ft/sec (m/sec)

X   distance, ft (m)

x   quality of mixture

α absorptance

ϵ thermal emittance

ν specific volume, ft^3/lb_m (m^3/kg)

σ surface tension, lb_f/ft (N/m)

τ period, sec

ρ density, lb/ft^3 (kg/m^3)

Subscripts:

b   boiloff

e   exit

f   final, force

g   gas

i   initial

L   centerline

ℓ liquid

m   mixture, mass

s   solar absorbtance of tank

t   thermal absorbtance of tank

v   vented gas

PROPELLANT MANAGEMENT

Considerable work had been done in the area of near-zero-gravity or low-gravity fluid mechanics in drop tower facilities, airplane flights, and small sounding rockets. A summary of this work is presented in reference 1. The studies generally indicate that the criteria for propellant retention and control is dependent on the Bond number, an expression involving the ratio of acceleration force to capillary force. The minimum acceleration required is determined by the critical Bond number, a value that can be determined both analytically and experimentally. A plot of minimum vehicle acceleration required as a function of tank diameter for ethyl alcohol is shown in figure 3. Since the surface tension to density ratio of ethyl alcohol closely approximates that for liquid hydrogen, figure 3 is also applicable for liquid hydrogen. For the Centaur vehicle, a minimum vehicle acceleration of 10^{-6} g was considered necessary for propellant control

(fig. 3). Propellant settling and retention through the application of an artificial gravitational field was the method chosen for Centaur.

AC-4 Propellant Management Problems

The AC-4 Centaur vehicle was launched to verify the adequacy of the Bond number provided for propellant control. AC-4 utilized a gravitational field created by two 2-pound (9-N) thrust propellant settling engines pointing aft. The settling engines were mounted on the aft end of the vehicle, as shown in figure 4, with the thrust vector applied through the expected vehicle center of gravity to minimize vehicle rotational torque. These engines, acting continuously throughout the coast period, provided a gravitational field of 3×10^{-4} g, which is two orders of magnitude greater than the predicted minimum requirement based on figure 3. The thrust from these engines, less the vehicle drag, provided a Bond number of about 240 for the hydrogen tank. This thrust appeared to be more than sufficient to retain the propellants at the bottom of the tanks. On the AC-4 flight, the 4-pound (18-N) thrust level proved to be insufficient to control the propellant disturbances created at main engine cutoff, resulting in liquid entrainment in the hydrogen vent flow. The impingement of the liquid-vapor mixture on the forward bulkhead of the vehicle in turn caused an unbalanced torque on the vehicle beyond the corrective capabilities of the control system, and the vehicle tumbled out of control.

Failure of the AC-4 flight to accomplish the coast phase portion of the mission clearly illustrated that low-gravity propellant management requires consideration of kinetic energies imparted to the liquid as well as the Bond number. The acceleration level used on AC-4 was not sufficient to suppress propellant disturbances.

AC-8 Propellant Management

Propellant management during the coast period requires the ability to control the propellant in a position which allows gas venting and supports a main engine restart. Successful management of the propellants during the coast phase depends upon the following:

(1) Identifying the source and determining the magnitude of energy imparted to the residual propellant in the tank at main engine shutdown and during the coasting period

(2) Providing means for dissipating the energy rapidly

(3) Retention of liquid in a location to allow venting of boiloff gas and liquid feed to the engine for restart

Analysis of AC-4 data indicate that energy may be imparted to the propellants during the boost phase, main engine cutoff, coast phase, or engine restart and may consist of any of the following:

(1) Pump backflow and return flow

(2) Pressurization gas flow impingement on liquid surfaces

(3) Propellant sloshing

(4) Propellant convective currents

(5) Unbalanced gas venting

(6) Attitude control engine firings

(7) Structural relaxation upon thrust termination

These energies in the liquid hydrogen tank are shown pictorially in figure 5. Energy dissipation can be accomplished with baffles and energy dissipators. Proper retention of liquid to allow venting can be accomplished by a series of properly selected thrust schedules to accomplish propellant suppression and retention during the coast period.

In the subsequent sections of the report, each kinetic energy source is treated separately. An analysis of each problem area, the problem disposition and a discussion of the successful AC-8 flight results are presented.

Energy Inputs to Propellant

The use of a pump to discharge cryogenic fluids from a space vehicle tank could introduce a large kinetic energy input to the fluid. The energy input results from pump bleed flow requirements to permit the pump to operate at zero discharge flow without cavitation. Also energy inputs can result from return flows designed to remove gases trapped in the propellant ducts downstream of the pump.

Volute bleed line flow. - In the Centaur hydrogen tank, a boost pump is used to discharge hydrogen from the tank and provide Net Positive Suction Head (NPSH) for the main engine turbopumps. This pump is provided with a volute bleed line (fig. 6), which bleeds fluid from the pump and allows it to operate at zero discharge flow without cavitation. The fluid is returned to the tank through a 2.0-inch-diameter (0.05-m-diam) line and is directed toward the forward end of the vehicle.

At engine shutdown, the power supply to the turbine drive is terminated, but the pump and turbine continue to rotate because of their own inertia. During the period in which pump speed decays from full speed to zero, fluid is continuously being returned to the tank. On AC-4, the volute bleed flow at main engine cutoff impinged on the forward bulkhead about 18 feet (5.5 m) away. A portion of this liquid was trapped in the hydrogen

tank vent exit, partially accounting for the liquid venting and subsequent vehicle tumbling (ref. 4).

Another effect associated with the liquid hydrogen boost pump volute bleed flow was also noted on AC-4 at the attempted second main engine start. Prior to main engine ignition, the boost pump was required to attain full speed in a zero discharge flow mode of operation. The volute bleed sprayed into the forward end of the tank, resulting in cooling of the ullage gas and subsequent reduction in ullage pressure. This reduction in ullage pressure decreased the available net positive suction head below the minimum required for satisfactory boost pump operation. The kinetic energy level of the liquid hydrogen boost pump volute bleed flow on the AC-4 flight was estimated to be 102 foot-pounds (139 J) (ref. 4).

To reduce the kinetic energy and prevent liquid spray into the ullage, an energy dissipator was designed and installed on this line on the AC-8 vehicle.

The design concept of the dissipator was to cause the fluid to undergo a constant enthalpy process in order to convert the kinetic energy into heat. This process is shown on a temperature-entropy diagram in figure 7. The line from A to B represents the pressure increase (work done on the fluid) through the boost pump, while the line from B to C to D represents the flow through the energy dissipator ending at some quality mixture entering the tank. This two-phase mixture results in a lower effective density, and when combined with the increased exit area of the energy dissipator, results in a reduced exit velocity.

Design and installation details of the volute bleed energy dissipator are shown in figures 8(a) to (c). The cross-sectional area of the dissipator was made elliptical because of installation and clearance requirements. The perforated plates were installed to dissipate the kinetic energy in a short distance and to maintain full flow in the dissipator. Data for head loss coefficients for orifices in constant area ducts were used in selecting the perforated plates. These data were applied by treating each hole in the plate as an orifice unaffected by the neighboring orifices. For the final plate design of 63 percent open area, the loss coefficient was 0.21.

Coincident with the design and installation of the volute bleed energy dissipator, two extensive ground test programs were initiated to reduce (1) the volute bleed flow rate to a minimum acceptable value and (2) the liquid hydrogen boost pump speed in response to decreased Centaur main engine turbopump net positive suction head requirements. These two programs resulted in reducing the liquid hydrogen volute bleed flow rate during steady-state operation from 340 gallons per minute (2.1×10^{-2} m^3/sec) on AC-4 to 65 gallons per minute (4.1×10^{-3} m^3/sec) on AC-8.

The calculated energy level of the total fluid discharged from the volute bleed line energy dissipator after first main engine cutoff was 0.32 foot-pound (0.43 J) on AC-8 compared to 102 foot-pounds (139 J) on AC-4.

Figure 9 compares the predicted spray heights with data from the AC-8 flight. The spray height was calculated for a flow rate of 65 gallons per minute (4.1×10^{-3} m^3/sec). (See appendix B for assumptions and detailed calculations.) The flight data were obtained from tank skin temperature sensors and in-tank liquid-vapor sensors. (Instrumentation is discussed in appendix A.) A good correlation exists between the predicted spray height and flight data.

AC-8 flight data verified the design concept of the volute bleed line energy dissipator. Figure 10 shows a comparison of AC-4 and AC-8 hydrogen tank ullage pressures prior to main engine restart. On AC-4, the pressure dropped very rapidly from the cooling effect of the volute bleed flow. On AC-8, no pressure drop was experienced with liquid hydrogen boost pump net positive suction head requirements being adequately met.

Recirculation line flow. - In the Centaur vehicle, a liquid hydrogen duct recirculation line, also shown in figure 6, is used to remove gas trapped at a high point in the hydrogen feed duct prior to main engine start. This recirculation ensures that the fuel ducts are chilled and filled with liquid, prior to main engine start.

Similar to the volute bleed line, the recirculation line also returns fluid to the tank during the period after main engine cutoff when the pump speed is decaying from full speed to zero. This also occurs prior to second main engine start while the pump is operating at zero discharge flow. The return line enters the tank at a point about 3 feet (0.9 m) directly above the volute bleed line, which is also below the liquid level at first main engine cutoff. The flow from this line is directed laterally across the tank. On the AC-4 flight, this flow probably also contributed to the decrease in ullage pressure at the attempted second engine start. At this time, the liquid level had decreased to a point below the recirculation line inlet to the tank, and the liquid flowed directly into the ullage.

The energy level of the flow from the hydrogen duct recirculation line on the AC-4 flight was estimated to be 35 foot-pounds (47 J). For the AC-8 flight, this level was reduced to a calculated value of 0.45 foot-pound (0.61 J) by installation of the energy dissipator shown in figures 8(a), (b), and (d). The design concept used here is the same as that of the volute bleed energy dissipator. The fluid is caused to undergo a constant enthalpy process and kinetic energy is converted to heat. The perforated plate hole sizes were selected by again applying data for orifice loss coefficients in constant area ducts.

The operation of the energy dissipator on the AC-8 flight was assumed to have been satisfactory, since no liquid disturbances were noted by the instrumentation on the tank wall opposite the return line.

Pressurization gas flow impingement on liquid surfaces. - Many space vehicles require gas pressurization to provide adequate net positive suction head for pump operation. If introduced into the tank improperly, the pressurizing stream can create large cavities in the liquid surface and cause splashing into the ullage (ref. 5). Splashing

8

could cause a drop in tank pressure by cooling the ullage, resulting in a loss in net positive suction head and possible boost pump cavitation prior to engine start. In the Centaur propellant tanks, pressurization is accomplished by injection of helium into the ullage.

Calculations for AC-4 hydrogen tank helium pressurization configuration (see fig. 11(a)) showed that the kinetic energy of the incoming gas into the hydrogen tank was 8.2×10^3 foot-pounds (11×10^3 J). In order to preclude the transfer of this energy to the liquid hydrogen in the form of splashing or sloshing, an energy dissipator was designed and installed on AC-8. The energy dissipator reduced the kinetic energy of the incoming pressurization gas to about 15 foot-pounds (20 J) at the dissipator exit.

The installation and design of the energy dissipator is shown in figure 11(b). The dissipator was required to reduce the kinetic energy of the flow so that splashing of the liquid surface would not occur. Two principal problem areas had to be overcome to maintain full flow in the dissipator. The first was that the flow area increase had to be in the order of 350 to 1 and had to be accomplished in a short distance. The second was that sonic velocities could exist in the pressurization line leading to the dissipator. To solve the first problem, perforated plates were used to dissipate the kinetic energy. These were chosen by applying loss coefficients for orifices in constant area ducts. The plates were formed to a 6-inch (0.15-m) spherical radius to provide structural strength. The second problem was solved by providing a small plenum with a high-pressure drop at the dissipator inlet. This partially relieved the area increase problem since an increase of about 10 to 1 was achieved here. Finally, the cone and plates were designed to have a small pressure loss (≈ 1 psia or 7×10^3 N/m^2) and an area increase of about 34 to 1.

Satisfactory operation of the energy dissipator on AC-8 was evidenced by the tank ullage pressure and internal tank instrumentation (see fig. 10).

Propellant sloshing. - Propellant sloshing is defined as back and forth and rotational wave motions of the free surface of a fluid in a partially filled tank. The wave height of the sloshing mass depends upon tank geometry, propellant properties, depth of propellant in the tank, acceleration field, and the magnitude and extent of coupling of the energies imparted to the fluid. The slosh wave height must be controlled in order to assure that no liquid reaches the tank vent exits. The slosh damping, or control, must account for the following:

    (1) The energy in the liquid due to sloshing initiated during the boost phase of the flight

    (2) The energy imparted to the liquid due to main engine cutoff transients

    (3) The energy imparted to the liquid from attitude stabilization control pulses, unbalanced tank vent forces, and thermal convective currents

In the transition from high to low vehicle acceleration that occurs at main engine cutoff, the amplitude of a residual slosh wave may be increased. The maximum in-

crease, or magnification, of the slosh wave amplitude will occur when the transition from high to low acceleration coincides with the time of maximum kinetic energy in the fluid (maximum wave velocity). The magnification factor M can be written

$$M = \left(\frac{\text{High acceleration level}}{\text{Low acceleration level}}\right)^{1/2} = \left(\frac{a_{hi}}{a_{lo}}\right)^{1/2}$$

The AC-4 magnification factor from main engine cutoff (2.44 g's) to the coast phase (3.0×10^{-4} g) was 90. Vehicle and propellant dynamic analyses have indicated that a slosh wave amplitude of 0.4 foot (0.12 m) prior to main engine cutoff represented the worst expected liquid hydrogen disturbance. With the magnification factor of 90 for AC-4, this disturbance could result in a slosh wave amplitude of approximately 36 feet (11 m). A slosh wave of this magnitude would completely encircle the liquid hydrogen tank since the top of the tank is about 14 feet (4 m) above the liquid level at first main engine cutoff. The slosh wave would also persist for the entire coast period since the slosh period at 3×10^{-4} g is approximately 120 seconds long and no means of slosh damping exists in the liquid hydrogen tank other than the tank itself.

In order to control the propellant disturbances at first main engine cutoff and to retain the propellants at the rear of the tanks throughout the coast period, the following approach for propellant control was established for the Centaur vehicle:

(1) A propellant settling period, provided by a short-term high-level thrust, was applied after first main engine cutoff to reduce the large magnification factor.

(2) A slosh baffle was added to the liquid hydrogen tank to dampen any slosh waves developed during the high-level thrust period when the slosh period will be of short duration.

(3) At the termination of the propellant settling period, a long-term low-level thrust was applied to the vehicle large enough to retain the propellants at the rear of the tanks.

(4) Another short-term high-level thrust was applied to the vehicle prior to second main engine start in order to suppress any disturbances associated with the second main engine start sequence.

For AC-8, a propellant settling phase of 100-pound (450-N) thrust, which resulted in an acceleration field of 7.5×10^{-3} g, was provided for 100 seconds after main engine cutoff. The 100-pound (450-N) thrust level was chosen to reduce the slosh wave height magnification factor to 18 at first main engine cutoff. This factor would result in a maximum slosh wave height subsequent to main engine cutoff of less than 8 feet (2.4 m), which is approximately 6 feet (1.8 m) below the tank vent exits.

At the termination of the 100-pound (450-N) thrust, a 6-pound (27-N) propellant retention thrust was applied during the coasting period until 46 seconds prior to second

main engine start. The 6-pound (27-N) thrust provided a vehicle acceleration of 4.5×10^{-4} g and a vehicle Bond number of 360. The Bond number of 360 was shown by scale-model testing (ref. 1) to be more than sufficient to retain the propellants at the rear of the tank and to maintain a flat liquid-vapor interface.

Forty-six seconds prior to the second main engine start, the 100-pound (450-N) thrust was again applied in order to suppress propellant disturbances (such as the volute bleed flow and pressurization gas impingement) associated with the second main engine start sequence. The complete AC-8 coast phase thrust schedule is shown in figure 12. The location of the propellant suppression and retention engines is shown in figure 13.

The magnification factor for the transition from the propellant settling phase to the 6-pound (27-N) thrust (4.5×10^{-4}-g) propellant retention phase is 4. If the 8-foot (2.4-m) slosh wave should persist through the propellant settling phase, a 32-foot (9.8-m) slosh wave would result in the propellant retention phase. Hence, the slosh waves resulting from the propellant disturbances that occur at main engine cutoff must be damped by a slosh baffle during the propellant settling phase to assure that the slosh wave amplitude is sufficiently small to prevent liquid from entering the vent exits at the transition to the propellant retention phase. Once the transition to the propellant retention phase is accomplished, the 6-pound (27-N) thrust will be sufficient to retain the liquid hydrogen at the rear of the tank.

For the liquid oxygen tank, no slosh baffle was added since the internal hardware inherent in the design of the Centaur vehicle served as effective baffles to dampen out propellant disturbances. Experimental investigation performed on a scale-model Centaur liquid oxygen tank verified that adequate damping was provided by the internal structures (ref. 6).

The slosh baffle configuration chosen for the Centaur liquid hydrogen tank is shown in figure 14. The baffle consists of a channeled ring, 12 vertical antiswirl baffles, and 3 bracket supports. The baffle was located just below the probable liquid level at first main engine cutoff. Prior to the launch of AC-8, slosh tests were performed in a scale-model Centaur liquid hydrogen tank (ref. 7). Scaling parameters used in the test were chosen so that the ratio of the gravitational to inertial forces (Froude number) was the same as for the full-size Centaur. The damping afforded by the slosh baffle was shown to be more than an order of magnitude greater than the damping afforded by an unbaffled tank configuration. A comparison between the baffle damping and the damping provided by the unbaffled tank on the maximum slosh wave height is shown in figure 15. The two curves for the baffled tank represent the maximum and minimum damping limits which are dependent on the liquid level at first main engine cutoff. As shown by these curves the maximum slosh wave amplitude subsequent to the termination of the propellant settling phase is about 3 feet (0.9 m) for the baffled tank (based on scale-model testing, ref. 7). This height compares with a maximum slosh wave of about 27 feet (8 m) (wave

height at propellant settling phase termination multiplied by the magnification factor of 4) for the unbaffled tank configuration. For AC-8, the effectiveness of the slosh baffle in damping propellant disturbances is indicated by the decreasing wave height values.

In AC-8, the slosh baffle, together with the 100-pound (450-N) propellant settling thrust, significantly reduced the liquid hydrogen disturbances. The instrumentation used in evaluating the propellant behavior during coast is discussed in appendix A. At first main engine cutoff, the liquid hydrogen tank was filled to a depth ratio (liquid depth/tank diameter) of approximately 0.67 (ref. 8). The liquid level was approximately 4 inches (0.1 m) above the slosh baffle. The location of the liquid level with respect to the slosh baffle and the level of the sensing elements of the liquid-vapor sensors is shown in figure 16. As indicated by this schematic, the liquid hydrogen can undergo oscillations of approximately 1 foot (0.3 m) without the liquid surface activating the level sensing instrumentation. On AC-8, the disturbances and reduction in acceleration that occurred at the termination of the propellant settling phase (100-pound (450-N) thrust termination) did not result in a slosh wave of sufficient magnitude to activate the liquid level sensing instrumentation.

From the 100-pound (450-N) thrust termination until 817 seconds into the propellant retention phase, the two 3-pound (13-N) thrust settling engines provided an acceleration of 4.5×10^{-4} g to maintain the liquid hydrogen at the rear of the tank. During this period no liquid motion was indicated by the level sensing instrumentation. At 817 seconds into the propellant retention phase, two of the settling engines no longer responded to the firing commands and failed to provide the proper settling thrust. In order to maintain vehicle attitude, the 50-pound (220-N) thrust engines were again commanded to fire intermittently by the autopilot. The reduction in acceleration resulting from the settling engine failure, together with the disturbances of the 50-pound (220-N) thrust engine firings, created a propellant sloshing condition which persisted throughout the remainder of the coast. During the remainder of the propellant retention phase, four distinct slosh waves were detected by the liquid-vapor sensors. A discussion and analysis of the four slosh waves is presented in appendix C. The wave profiles of the four slosh waves, at the times of various liquid-vapor sensor activations, are presented in figures 31 to 34. The analysis indicates that the slosh baffle was primarily responsible for preventing the slosh wave amplitudes from reaching the tank vent exits and further demonstrates the effectiveness of the AC-8 slosh baffle in controlling propellant sloshing disturbances.

Other energy sources. - In the general treatment of propellant management, some sources of energy cannot be treated directly in the same manner as the volute bleed flow energy or the pressurization gas energy. These energies must be evaluated and, if found significant, an attempt made to dissipate the kinetic energy. This section deals with three energy sources evaluated in the Centaur vehicle.

Intermediate bulkhead springback: During powered flight, the intermediate bulkhead

is deflected by propellant loads in response to the increasing acceleration field in a manner analogous to a spring being compressed. The deflection stores strain energy in the bulkhead. Upon thrust termination at main engine cutoff, the structure returns to its undeflected position, transmitting the stored energy to the liquid. The energy level on AC-4 was calculated to be 0.12 foot-pound (0.17 J) (ref. 4), which was less than a tenth of a percent of the total kinetic energy input to the fluid on AC-4.

Propellant line surge: During main engine firing, propellant is transported to the engines through the feed lines at a high velocity and at a pressure level higher than the tank pressures. At main engine cutoff, the propellant flow to the engines is terminated by rapid closing of the main engine inlet valves. The fluid momentum causes the propellant flow to reverse direction and surge back into the tank. The energy level from pump back flow on AC-4 was calculated from ground test data (ref. 4) to be 35 foot-pounds (47 J) which was less than 17 percent of the total kinetic energy input to the fluid on AC-4.

Thermal convective current: During powered flight, thermal convective currents are established in the boundary layer of the fluid because of absorption of thermal energy. At main engine cutoff, the vehicle acceleration is suddenly reduced. Calculations show that the boundary layer would continue to move forward in the tank. The energy level on AC-4 was calculated to be 1.1 foot-pounds (1.5 J) (ref. 4), which was less than 1 percent of the total kinetic energy input to the fluid on AC-4.

Since the energies involved from the intermediate bulkhead springback, propellant line surge, and thermal convective currents are small and difficult to treat directly, the slosh baffle and thrust schedule discussed previously were designed to dissipate the sum of these three propellant energies in addition to the energy from slosh caused by external vehicle forces.

An examination of AC-8 flight data verified the design concept of the baffle, thrust schedule, and energy dissipators. The disturbances induced at first main engine cutoff were quickly dissipated by the slosh baffle. The height of the volute spray was kept well below the vent exits such that venting of the hydrogen tank was satisfactorily accomplished. The tank pressure in the hydrogen tank stayed near the predicted values, supplying the net positive suction head required by the boost pump for second main engine start.

Propellant Heating and Tank Venting

In addition to an accounting of the kinetic energy, the proper management of a cryogenic fluid in a coast phase also requires an accounting of the thermal energy imparted to the fluid. The thermal energy absorbed by a cryogenic fluid will result in liquid boil-

off and a subsequent rise in tank pressure.

Thermal energy from the space environment consists of solar energy, reflected solar energy from the Earth-atmosphere system (albedo), long wavelength energy radiated from the Earth-atmosphere system by virtue of its temperature (Earth-thermal radiation), and free molecular aerodynamic heating. In order to establish the adequacy of preflight thermal analyses of the amount of boiloff and tank pressure rise expected to occur during coast, a liquid hydrogen tank internal and external thermal survey was performed on AC-8.

AC-8 thermal energy input. - The external space energy fluxes (solar, albedo, Earth thermal, and aerodynamic) were determined by banks of selectively absorbing calorimeters. Five calorimeter banks were employed on AC-8. The locations of these calorimeter banks, with respect to the Centaur liquid hydrogen tank, are shown in figure 17. A discussion of the calorimeters, together with the measurements of the individual energy fluxes, is presented in appendix D.

The thermal heat flux to the Centaur liquid hydrogen tank during the coast phase is plotted in figures 18 and 19. The arithmetic average heat flux is represented by the dashed line. The curves reflect the vehicle motion experienced during coast. The coast phase of AC-8 was completed in the Earth's shadow (solar radiation and Earth albedo were not present); hence, the heat fluxes shown in figures 18 and 19 are representative of minimum space heating for coast flight at this altitude.

The thermal history of the interior of the Centaur liquid hydrogen tank was provided by a system of tank temperature sensors, located as shown in figure 20. The operation and design of these sensors are discussed in appendix A. The tank ullage temperature profiles indicated by the sensors are presented in figure 21. As indicated by these profiles, the heating of the liquid hydrogen tank ullage resulted in the formation of stratified layers. These layers were established by the forward movement of mass and heat in a convective layer on the inner surface of the tank skin. No satisfactory analytical prediction of their formation has been established. On AC-8, temperatures varied from 40° R (22° K) at the liquid surface to 140° R (78° K) at the forward end of the tank. The temperature sensors showed that there were no significant radial and circumferential temperature gradients.

To complete the thermal survey of the liquid hydrogen tank on the AC-8 mission, the liquid hydrogen tank skin, was instrumented with 45 external tank skin temperature sensors. The sensors were symmetrically located on the tank as shown in figure 22. The skin temperatures enabled the determination of the amount of heat that is reradiated from the tank.

The thermal energy absorbed by the cryogenic fluid can be determined when the tank skin temperatures, the liquid and gas temperatures, and the external heat fluxes are known. The heating rates to the Centaur liquid hydrogen, and to the tank ullage,

14

are presented in figures 23 and 24. On the basis of these heating rates, the amount of liquid hydrogen boiloff, the tank ullage temperature increase, and the tank pressure rise rate were calculated for the AC-8 mission (appendix D).

Propellant tank vent system. - In order to maintain the tank pressures within structural limits, gaseous hydrogen must be discharged from the tank.

The AC-4 coast phase hydrogen vent system is shown in figure 25. The system consisted of a standpipe, venturi flow meter, two parallel vent valves, and a plenum with opposing exits in the vehicle pitch plane. Gaseous hydrogen flow from the tank through the standpipe was measured by the venturi. Hydrogen tank pressure was regulated by the lower range vent valve (20.5 psia or 1.4×10^5 N/m^2) during coast, with the upper range valve (26.5 psia or 1.8×10^5 N/m^2) acting only in the safety relief mode. During boost, vent flow was directed through a vent stack located on the nose fairing as shown. At nose fairing jettison, the ducting from the plenum to the vent stack and a cap on the opposing side were disconnected, allowing venting through the plenum exits. With normal gaseous flow the unbalanced torques produced by gas impingement on the forward end of the tank were within the vehicle attitude control capability. However, the propellant disturbances at main engine cutoff resulted in the entrainment of liquid hydrogen which impinged on the vehicle and produced a torque in excess of the control capability of the attitude control engines. As a result, the vehicle tumbled causing further liquid venting. Venting should therefore be accomplished in either a nonpropulsive (thrust cancelling) mode or with the vent gases directed symmetrically in the aft direction. The nonpropulsive method has been chosen for Centaur.

AC-8 coast phase vent system. - In conjunction with the installation of the energy dissipators and baffle in the AC-8 hydrogen tank, a new balanced thrust vent system was designed and installed. The AC-8 vent system design is shown in figure 26. The primary design objective of the AC-8 vent system was to provide nonpropulsive, nonimpingement gas venting during the coast phase.

The liquid hydrogen boiloff gases were vented out of the top of the tank through the valves and into a torus assembly. The flow was then discharged radially in opposite directions. Convergent nozzles were installed at the duct exits, which were located as far outboard as practical, to provide flow limiting control and to act as a flowmetering device. A deflector plate was inserted below the duct inlet to prevent liquid from sloshing directly into the vent line. The torus was designed symmetrically to minimize any unequal flow splitting at the vent valve discharge and to provide pressure equalization at the exit nozzles for thrust cancellation.

Balanced thrust performance of the vent system was verified by extensive ground testing. For maximum steady-state gas venting conditions of 0.6 pound per second (0.3 kg/sec) encountered in Centaur, the thrust unbalance was 0.15 pound (0.67 N). This was well within the attitude control capability.

Vent system thrust unbalance during the coast phase depends upon the amount of the liquid hydrogen boiloff. The AC-8 coast phase took place in the Earth's shadow and resulted in a very low heat flux to the liquid hydrogen tank. The vehicle disturbances resulting from the venting cycles were very minor requiring no detectable attitude control correction.

The measured vent flow indicated that a total of approximately 5.2 pounds (2.4 kg) of gaseous hydrogen was vented during the coast period. A calculation of the vented gas quantity from the absorbed thermal energy yields 5.1 pounds (2.3 kg) of gaseous hydrogen as the vented quantity (appendix D). The calculated liquid hydrogen tank pressure rise rate of 0.46 pound per square inch per minute (53 $N/(m^2)(sec)$) compared favorably with the actual pressure rise rate of 0.48 pound per square inch per minute (55 $N/(m^2)(sec)$). These comparisons indicated that a satisfactory accounting of the thermal energies had been accomplished for the Centaur vehicle.

CONCLUSIONS

For lunar and deep space missions, a versatile space vehicle should posses the capability to restart the engines after a coasting period in space. In order to fulfill this requirement for an orbiting space vehicle, the propellant behavior must be defined and the method of control must be established. The flight of the fourth Atlas-Centaur (AC-4) vehicle indicated that the propellant behavior in a full-scale space vehicle cannot be properly defined solely by the consideration of the Bond number. The definition of the propellant behavior requires a complete accounting of the energy inputs to the fluid as well. For a cryogenic fluid in a space vehicle, the energy inputs may consist of one or more of the following sources:

(1) Pump backflow and return flow
(2) Pressurization gas flow impingement on the liquid surface
(3) Residual propellant sloshing
(4) Propellant convective currents
(5) Unbalanced thrust from gas venting
(6) Attitude control engine firings
(7) Structural relaxation at the time of thrust termination

All of these energy sources are present in the Centaur vehicle.

Various methods, developed for the control of the kinetic energy inputs, were employed during the flight of the eighth Atlas-Centaur vehicle. As a result of the flight, the following conclusions concerning the management of a cryogenic fluid in a full-scale orbiting space vehicle were obtained:

1. The kinetic energy imparted to the propellant by the pump volute bleed flow, duct

recirculation line return flow, and the tank pressurization gas flow were reduced to acceptable levels by employing energy dissipation devices.

2. The propellant disturbances that occur at thrust termination were greatly reduced by a controlled schedule of thrust levels when combined with the addition of a slosh baffle in the tank.

3. The vent system should be designed to minimize venting disturbance torques on the vehicle. The propellants in the tanks must also be properly positioned to assure that liquid is not vented overboard. Venting of liquid may not only deplete the propellants but it may also produce large unbalanced torques on the vehicle.

The flight of the eighth Atlas-Centaur vehicle clearly demonstrated a method for control of a cryogenic fluid in a full-scale orbiting space vehicle. The method of propellant control established for the Atlas-Centaur is applicable to any space vehicle that entails the short-term storage and use of cryogenic propellants.

Lewis Research Center,
    National Aeronautics and Space Administration,
        Cleveland, Ohio, September 7, 1967,
           891-01-00-06-22.

APPENDIX A

INSTRUMENTATION FOR PROPELLANT MANAGEMENT

The eighth Atlas-Centaur (AC-8) vehicle was extensively instrumented to observe propellant behavior during the coast period. The instrumentation is enumerated as follows:

(1) Thirty-two liquid-vapor sensors to detect liquid slosh motion and other liquid disturbances in the hydrogen tank

(2) Sixteen temperature sensors to determine the temperature distribution in the hydrogen tank ullage

(3) Forty-five temperature sensors to measure the hydrogen tank skin temperature (The temperature sensors also act as detectors of liquid slosh motion at the tank wall.)

(4) An absolute pressure transducer and a vent gas temperature sensor in each of the two balanced vent nozzle inlets to allow calculation of the quantity of hydrogen vented during the coast phase; also, a differential pressure transducer to measure any pressure difference across the nozzle inlets to determine any thrust unbalance due to unequal pressures at the nozzle inlets

(5) Five calorimeters in the forward area of the vehicle to measure incident heat flux to the vehicle during the coast period

(6) Two low-gravity accelerometers to measure vehicle axial accelerations as a result of the propellant settling and retention thrusts (Accelerations perpendicular to the vehicle axes were also measured to detect vehicle disturbances in these directions.)

(7) Four pressure transducers to monitor both liquid hydrogen and liquid oxygen tank pressure histories throughout the coast period

The liquid oxygen tank was instrumented with 4 tank skin temperature sensors and 4 ullage temperature sensors. Instrumentation in the oxygen tank was less extensive because the area of primary concern was the hydrogen tank.

Liquid-Vapor Sensors

The liquid-vapor sensors were distributed in the hydrogen tank as shown in figure 20. The liquid-vapor sensor, shown in figure 27, consists of a conical tip, in which a germanium temperature sensing element is located, and a cylindrical body. Within the cylindrical body is housed a heater (0.3 W), a current limiting resistor, and associated wiring and insulation. When the sensor is immersed in liquid, heat generated by the heater

18

is conducted away from the tip by the liquid, causing the resistance sensor to indicate approximate liquid temperature. The signal produced by this condition is interpreted as the presence of liquid. When the sensor is in vapor, heat generated by the sensor is not conducted away as rapidly, thereby causing the temperature of the sensing tip to rise. The increase in temperature causes a decrease in the germanium sensor resistance which is interpreted as the absence of liquid.

The liquid-vapor sensor used in AC-8 was specifically designed for a wetting liquid (contact angle less than 90°) in a low-gravity environment. Because of its extremely low surface tension, liquid hydrogen possesses a zero-degree contact angle on all known solid surfaces. In a low-gravity field, liquid hydrogen will tend to spread over solid surfaces to satisfy the condition of minimum total energy. Sensors designed for normal gravity operation are generally inoperative in low-gravity environment because they always tend to indicate liquid. Studies and tests conducted at the Lewis Research Center have shown that surface tension will cause a wetting liquid on a conical surface to move in the direction of increasing radius (i.e., the base of the cone) in a low-gravity environment (ref. 9). The liquid motion due to surface tension is utilized in the liquid-vapor sensor to uncover the sensing element located at the conical tip.

The response characteristics of a typical liquid-vapor sensor from the AC-8 flight as compared with ground test response characteristics are shown in figure 28. The ground test characteristics were obtained from tests performed by the National Bureau of Standards at Boulder, Colorado. The flight data compared favorably with the ground test results. The time response of the sensors is adequate for the application for which they are intended. During the coast phase, the slosh period in the AC-8 hydrogen tank was about 23 seconds for the propellant settling period and 100 seconds for the propellant retention period.

Ullage Temperature Sensors

The ullage temperature sensor assembly shown in figure 29 consists basically of a conical germanium or platinum temperature sensor and an insulating body which, in this instance, is conically shaped. This sensor is a resistance-type sensor with either platinum or germanium as the sensing element. The germanium sensor has a temperature range of 40° to 120° R (22° to 67° K), while the platinum sensor has a temperature range of 40° to 190° R (22° to 106° K). The heater assembly used in the liquid-vapor sensor is not incorporated into the temperature sensor. As with the liquid-vapor sensors, the sensing element is located near the conical tip in order to utilize the effect of surface tension to clear the surface of any residual liquid when the sensor is in vapor environment.

The location of the temperature sensors is shown in figure 20. The sensors are generally located above the expected liquid level during the coast period in order to measure the radial and axial temperature distribution in the ullage. The temperature sensors also serve as liquid detectors by showing a sudden drop in temperature when liquid is splashed into the warm ullage.

A comparison of sensor response time between flight data and ground test results performed by the National Bureau of Standards is shown in figure 30. The flight data agreed well with the ground test curve.

Tank Skin Temperature Sensors

The location of the external tank skin temperature sensors on the hydrogen tank is shown in figure 22. They were resistance-type sensors used extensively in industry. As with the internally mounted temperature sensors, the tank skin sensors were either of germanium or platinum element, depending on the range of temperature measured.

The tank skin sensors also serve to detect the presence of liquid by showing a sudden temperature drop as the warm tank skin comes in contact with the liquid.

Low-Gravity Accelerometer

A low-gravity accelerometer capable of measurement down to the order of 10^{-5} g was used to measure the vehicle acceleration during the coast phase of the flight. The accelerometer is a single-axis, pendulum, force rebalance instrument. The instrument, which consists primarily of a pendulum supported by two thin springs, is shown schematically in the following sketch:
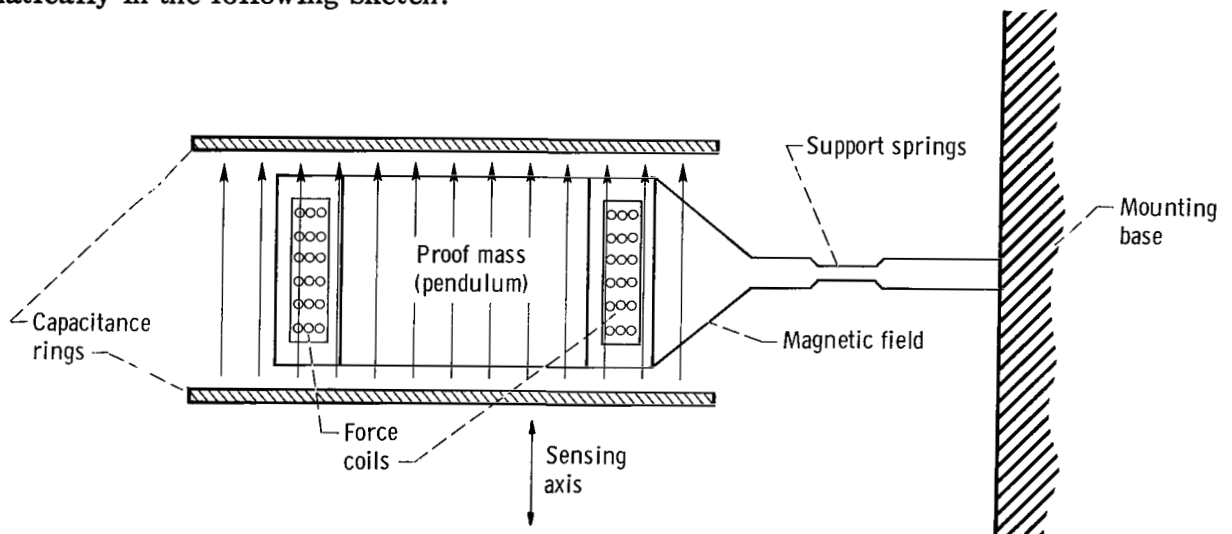
The pendulum is located in a magnetic field developed by a permanent magnet. The main mass of the pendulum contains the force coil and the center plate of a capacitance pickoff. The pickoff operates in a bridge circuit which provides an output proportional to the pendulum deflection. The bridge output is amplified, detected, and applied as d-c current to the force coil (located on the pendulum in the field of the permanent magnet) to electrically constrain the pendulum. Through the servo action, the force resulting from the current in the force coil balances the acceleration forces acting on the pendulum. The force coil current is then proportional to the applied acceleration. The current is measured by inserting a precision resistor in series with the force coil and measuring the voltage developed across the resistor.

The accelerometer was generally successful in measuring acceleration levels as low as 2.2×10^{-4} g experienced by the AC-8 vehicle.

APPENDIX B

VOLUTE BLEED ENERGY DISSIPATOR CALCULATIONS FOR AC-8

To determine the height to which the return flow from the liquid hydrogen boost pump volute bleed would spray into the tank at first engine shutdown, it was necessary to determine the velocity of the liquid stream as it left the liquid surface. Interaction between the volute bleed spray and the recirculation line flow was neglected. From reference 11, the velocity at any point in a submerged jet can be calculated from the following empirical equation:

$$\left(\frac{V_\ell}{V_e}\right)\left(\frac{X}{D}\right) = 6.4 \tag{B1}$$

where

V_ℓ velocity of stream as it breaks liquid surface

V_e velocity of stream at dissipator exit

X distance from dissipator exit to liquid surface

D diameter of circle with area equivalent to dissipator elliptical exit

After the liquid hydrogen leaves the boost pump, it is returned to the pressure in the tank. Therefore, the energy acquired from the pump is dissipated by vaporization of a portion of the liquid flow. If it is assumed that all power from the pump is converted into heat, then the heat generated per pound of liquid hydrogen is

$$\frac{Heat}{Pound\ fluid} = \frac{P}{\dot{M}} \tag{B2}$$

where

P pump power

$\dot{M}$ volute bleed mass flow rate

The amount of fluid vaporized then is

$$x = \frac{P}{\dot{M}h} \tag{B3}$$

where

h   heat of vaporization of hydrogen

x   quality or percent vaporized

The specific volume of a two-phase mixture can be calculated from

$$\nu_m = x(\nu_g - \nu_\ell) + \nu_\ell \tag{B4}$$

where

ν_m specific volume of mixture

ν_g specific volume of saturated gas

ν_ℓ specific volume of saturated liquid

Substituting x from equation (B3) into equation (B4) gives

$$\nu_m = \frac{P(\nu_g - \nu_\ell)}{\dot{M}h} + \nu_\ell \tag{B5}$$

Since the density of the two-phase mixture ρ_m is

$$\rho_m = \frac{1}{\nu_m} \tag{B6}$$

the velocity of the stream at the dissipator exit V_e can be calculated from the continuity equation as follows:

$$V_e = \frac{\dot{M}}{\rho_m A_e} = \frac{4\dot{M}}{\pi \rho_m D^2} \tag{B7}$$

Substituting equation (B7) into equation (B1) yields

$$V_\ell = 6.4 \left(\frac{D}{X}\right) \left(\frac{4\dot{M}}{\pi \rho_m D^2}\right) = \frac{25.6\,\dot{M}}{\pi \rho_m DX} \tag{B8}$$

Equations (B6) and (B8) now enable calculation of the velocity of the stream as it breaks the liquid surface V_ℓ. For AC-8, the values are as follows:

Pump power, P, hp (W) . . . . 11 (8.2×10^3)

Mass flow rate, $\dot{M}$, lb_m/sec (kg/sec) 0.6 (0.3)

Enthalpy, h, Btu/lb_m (W/kg) . . . . .194 (4.5×10^5)

Specific volume of saturated gas, ν_g, ft^3/lb_m (m^3/kg) 7.6 (0.48)

Specific volume of saturated liquid, ν_ℓ, ft^3/lb_m (m^3/kg) 0.24 (0.15)

Diameter, D, ft (m) 0.56 (0.17)

Distance, X, ft (m) 51.5 (1.31)

Substitution of these values into equations (B6) and (B8), in proper units, yields a value for V_ℓ of 1.5 feet per second. The height of a particle in the stream after it leaves the liquid surface can be calculated from the equations of rectilinear motion and is shown in figure 9.

APPENDIX C

AC-8 PROPELLANT SLOSHING DURING THE PROPELLANT RETENTION PHASE

Irregularities in two of the four 3-pound (13-N) thrust propellant retention engines were noted at 917 seconds after first main engine cutoff (ref. 8). These engines failed to respond to the firing commands. Analysis of the flight data indicated that the engine failure resulted from a hydrogen peroxide propellant leak. As a result of this failure, the 50-pound (220-N) thrust engines were activated in an attitude control mode.

At 955 seconds after first main engine cutoff, a liquid vapor sensor, (1 foot (0.3 m) above the liquid surface) was activated, indicating the presence of a slosh wave. This slosh wave continued throughout the remainder of the coast period.

From 917 seconds to 1449 seconds into the propellant retention phase, four cyclic slosh waves were noted. These four slosh waves are presented in figures 31 to 34. The location of the liquid-vapor sensing instrumentation is presented in each figure to aid in correlating the actual data with the sloshing waves shown. Actual sensor activation data are presented in figure 35, together with an aft view schematic of the instrumentation arms at a liquid depth ratio of 0.75 and 0.50. The 50-pound (220-N) thrust engine firing times are also presented in this figure.

The first slosh wave, shown in figure 31, persisted for approximately 143 seconds. The probable wave profiles at the times of various liquid-vapor sensor activations are also presented in this figure. At 995 seconds after first main engine cutoff, the two remaining 3-pound (13-N) thrust retention engines were commanded to fire in order to provide attitude control. These engines fired sporadically for the remainder of the coast, resulting in alternating periods of 3-pound (13-N) thrust and the thrust provided by atmospheric drag. The acceleration levels experienced by the vehicle during the propellant retention phase are presented in figure 36. The average acceleration level was determined by the equation

$$a\text{(average)} = \frac{1}{\tau} \int a \, dt$$

The average acceleration level during the first slosh wave was 7.4×10^{-5} g. The average wave velocity (distance between sensors divided by the time between sensor activations) of the first slosh wave was about 0.3 inch per second (8×10^{-3} m/sec).

The second slosh wave began at about 1063 seconds after first main engine cutoff and persisted for approximately 129 seconds. The probable wave profiles at three liquid-vapor sensor activations are shown in figure 32. Both sensors at the 0.75 depth ratio quadrant IV arm were activated at nearly the same time, indicating a relatively

flat wave profile in this quadrant. The average vehicle acceleration level during the second slosh wave was about 1.1×10^{-4} g. The average wave velocity was about 0.5 inch per second (1×10^{-2} m/sec).

The third slosh wave began at about 1193 seconds after first main engine cutoff and persisted for approximately 122 seconds. The probable wave profiles at the two liquid-vapor sensor activation times are shown in figure 33. The inner sensor on the 0.75 depth ratio quadrant IV arm did not activate, indicating that the amplitude of the third slosh wave was not as large as the amplitude of the two previous slosh waves. The average acceleration level for the third slosh wave was about 8.9×10^{-5} g. The average wave velocity was approximately 0.3 inch per second (8×10^{-3} m/sec).

The fourth slosh wave began at about 1316 seconds after first main engine cutoff and persisted for approximately 133 seconds. The probable wave profiles at the times of three liquid-vapor sensor activations are shown in figure 34. The sensor on the longitudinal axis at the 0.538 depth ratio was activated briefly resulting in the break in slope shown for the wave profile at 1300 seconds into the propellant retention phase. The average acceleration level during the fourth slosh wave was about 1.2×10^{-4} g. The average wave velocity was about 0.4 inch per second (1×10^{-2} m/sec).

The pertinent aspects of the four slosh waves are presented in the following table

Slosh wave	Actual slosh period, sec	Average wave velocity		Average acceleration level, g	Calculated slosh period, sec	Bond number, $\rho r^2 a/\sigma$
		in./sec	m/sec			
1	143	0.3	8×10^{-3}	7.4×10^{-5}	240	64
2	129	.5	1×10^{-2}	1.1×10^{-4}	193	99
3	122	.3	8×10^{-3}	8.9×10^{-5}	219	76
4	133	.4	1×10^{-2}	1.2×10^{-4}	186	103

The calculated slosh period is determined from the equation

$$\tau = 1.66\ \pi\left(\frac{r}{a}\right)^{1/2}$$

(ref. 7), which is valid for Bond numbers greater than 50. The difference between the actual and the calculated slosh period is attributed to the slosh waves being initiated and continuously modified by the continued application of attitude control pulses.

The quadrant I and IV 50-pound (220-N) thrust engines fired 13 times each during the propellant retention phase. Analysis of the data presented shows that there is correlation of these firing times to the four sloshing waves. It appears likely that the 50-pound (220-N) thrust engine firings are responsible for initiating and sustaining the

sloshing condition, while correcting the attitude errors due to the peroxide leak. If it is assumed that the 50-pound (220-N) thrust engines initiated the sloshing, then an analysis can be made to determine if sufficient energy could be imparted to the fluid that would create slosh waves of the magnitudes observed in flight.

From the scale-model Centaur liquid hydrogen tank sloshing tests, mentioned previously, the quantities necessary to describe the sloshing as a pendulum analogy were obtained (ref. 7). These quantities were used to determine the energy imparted to the sloshing mass from the firing of the 50-pound (220-N) thrust engines. The firings imparted a lateral excitation of about 0.12 inch (3.1×10^{-3} m) to the sloshing mass, resulting in a kinetic energy input of 12 foot-pounds (14 J). Assuming that all of the energy went into producing liquid motion, the kinetic energy would produce a wave velocity of 2 inches per second (0.05 m/sec). The actual wave velocities varied from 0.3 to 0.5 inch per second (8×10^{-3} to 1×10^{-2} m/sec). The kinetic energy input to the liquid due to the 50-pound (220-N) thrust engine firings is more than sufficient to create the slosh wave magnitudes that occurred after the propellant retention engine failure. The majority of the difference between the calculated and the actual wave velocities can be attributed to the removal of kinetic energy from the liquid by the slosh baffle. The difference also indicates that the slosh baffle prevented the slosh wave from reaching the forward end of the liquid hydrogen tank.

From the analysis of the propellant retention phase sloshing that occurred on AC-8, the following conclusions were made:

(1) The sloshing condition was initiated by the 50-pound (220-N) thrust engine firings. These firings were necessitated by the failure of two propellant retention engines.

(2) Four, major slosh waves occurred during the propellant retention phase.

(3) The slosh waves were sustained and the wave shapes were modified by the 50-pound (220-N) thrust engine firings.

(4) The slosh baffle prevented a large wave velocity and a corresponding large wave amplitude which would have resulted in the slosh wave reaching the top of the liquid hydrogen tank.

APPENDIX D

CALCULATION OF CENTAUR LIQUID HYDROGEN TANK PRESSURE RISE

RATE AND VENTED QUANTITY

In order to establish the heat inputs to the Centaur liquid hydrogen tank necessary for the determination of the boiloff rates and tank pressure rise rates, five calorimeter banks were employed on AC-8 as shown in figure 17. Each calorimeter bank consisted of three asymptotic calorimeters. Each asymptotic calorimeter consists basically of a thin Constantan foil suspended over a cavity in a copper heat sink. The foil is thermally and electrically attached to the heat sink at the periphery of the cavity. A differential thermocouple is formed with the hot and cold junctions at the foil center and periphery, respectively. The temperature difference between the center and periphery of the foil is directly proportional to the heat flux over the surface of the foil.

The surface finish of each of the three asymptotic calorimeters was predominantly sensitive to thermal radiation in a different selected spectral region. The three surface finishes were black colloidal graphite, gold electroplate, and white enamel. The absorptance and emittance of each surface were established by ground tests as a function of the calorimeter temperature.

The calorimeter output was calibrated to the heat flux by ground tests in solar radiation simulators at both General Dynamics/Convair and the Lewis Research Center. By having three calorimeters with three different surfaces and, hence, three different outputs, three equations in four unknowns may be written at any given time in the coast phase for each calorimeter bank. Each equation will be of the following form:

$$\text{Calorimeter signal} \xrightarrow{\text{yields}} \text{net heat flux } (q_{net})$$

$$q_{net} = \alpha_s(q_{solar} + q_{albedo}) + \alpha_t q_{thermal} + q_{aero} - \epsilon q_{reradiation} \tag{D1}$$

The last term, the reradiation correction, was incorporated into the calorimeter calibration. A fourth equation results from knowledge of the vehicle orientation where at least one of the heat fluxes will be zero. The resulting series of four equations are then solved simultaneously to determine the four individual heat fluxes.

Since the AC-8 mission was completed in the Earth's shadow, only the Earth thermal radiation and aerodynamic heat fluxes were of significance. The Earth thermal radiation fluxes recorded by the four outward facing calorimeter banks during the coast period are presented in figure 37. The heat fluxes, as shown, provide a graphical representation

of the Centaur vehicle roll during coast. As the surface of a given calorimeter bank is rotated to face the Earth, the Earth thermal radiation recorded by the calorimeter bank increases from zero to a maximum of about 80 Btu per hour per square foot (250 W/m^2). The maximum predicted Earth thermal heat flux was 76 Btu per hour per square foot (240 W/m^2).

The free molecular aerodynamic heat flux recorded by the outward facing calorimeter bank varied from zero to 10 Btu per hour per square foot (315 W/m^2) with an average aerodynamic heat flux of 4.4 Btu per hour per square foot (13.9 W/m^2).

At the forward end of the Centaur liquid hydrogen tank, the aerodynamic heat flux provided the major source of space environmental heating. The free molecular aerodynamic heat flux, as well as the thermal radiation heat flux, recorded by the forward facing calorimeter bank are presented in figure 38. The maximum recorded aerodynamic heat flux was 57 Btu per hour per square foot (180 W/m^2). The predicted aerodynamic heat flux for the Centaur vehicle at its coast phase altitude of 90 nautical miles (1.67×10^5 m) was 66 Btu per hour per square foot (208 W/m^2). The free molecular aerodynamic heat flux decrease reflects the Centaur vehicle increase in altitude from 90 to 108 nautical miles during the coast period. The Earth thermal heat flux decrease reflects the roll of the Centaur vehicle during the coast period.

Once the individual space energy fluxes are known, the environmental heat flux for a given area of the Centaur liquid hydrogen tank in line with the calorimeters can be determined. The following equation may be used to define the heat flux to the stainless-steel Centaur liquid hydrogen tank side wall:

$$q_{net}(\text{tank wall}) = \alpha_s(\text{tank wall})\left(q_{albedo} + q_{solar}\right) + \alpha_t(\text{tank wall})q_{thermal}$$

$$+ q_{aero} - q_{reradiation} \qquad \text{(D2)}$$

The absorptance and emittance for the stainless-steel tank were established as functions of temperature by ground testing.

The reradiation term was negligible because of the low (97° R or 54° K) tank skin temperature experienced during the coast phase. The heat flux into the Centaur liquid hydrogen tank side walls at four longitudinal sections is shown in figure 18.

The heat flux into a given quadrant of the forward bulkhead of the liquid hydrogen tank was determined by averaging the energy fluxes measured by each of the outward facing calorimeter banks with the energy flux measured by the forward facing calorimeter bank. These fluxes, together with the appropriate radiation parameters for the bulkhead, were substituted into equation (D2). The resulting equation was then solved for the heat flux. The environmental heat fluxes into four longitudinal sections of the

forward bulkhead of the Centaur liquid hydrogen tank and their arithmetic average are presented in figure 19.

In addition to the space environment energy sources, the Centaur liquid hydrogen tank receives heat from two other major sources; they are the following:

(1) Radiation and conduction to the tank ullage from electronic components and pay-load adapter of 1100 Btu per hour (280 W)

(2) Conduction from liquid hydrogen boost pumps and feed lines and heat transfer through the intermediate bulkhead to the liquid hydrogen of 1200 Btu per hour (350 W).

These two heat inputs, together with the environmental energy inputs, constitute the total heat input to the Centaur liquid hydrogen tank during the coast period.

The heat rates to the liquid hydrogen are presented in figure 23. These rates represent the sum of the environmental heat flux to the tank side wall area in contact with the liquid, and the heat rate from the intermediate bulkhead and feed lines. The integration of these heat rates over the entire venting period yields 690 Btu (7.3×10^5 J) as the net heat input to the liquid hydrogen. This heat input would result in the vaporization of 3.6 pounds (1.7 kg) of liquid hydrogen.

A summary of the individual heat input rates to the Centaur hydrogen tank during the venting period are presented in figure 39. As shown, the environmental heating rates A' and C' are not entirely transmitted to the ullage. A small quantity of their heat input results in the heating of the tank wall mass, and a small quantity of their heat is re-radiated from the tank as a result of the tank wall temperature increase. During the venting period, the average tank skin temperature remained constant at about 97° R (54° K). At this temperature, the amount of heat reradiated from the tank wall was negligible. The heat rate to the Centaur hydrogen tank ullage are presented in figure 24. The integration of these heat rates over the entire venting period yields 1400 Btu (1.5×10^6 J) as the net heat input to the tank ullage.

At the initiation of the venting period (605 sec after first main engine cutoff), the average bulk temperature of the tank ullage was 54° R (30° K). This average increased to 55° R (31° K) by the end of the venting period. The total venting time was 51 seconds. These averages were obtained from the tank ullage temperature data previously presented.

The energy balance for the tank ullage during the venting period is given by the expression

$$Q = M_f U_f - M_i U_i + M_v h_v - M_b h_b \qquad \text{(D3)}$$

Calculation of the quantity vented from the energy balance yields 5.1 pounds mass (2.3 kg) as the amount vented. This compares very favorably with the measured quantity

of 5.2 pounds mass (2.4 kg) vented for the 850 seconds of the venting period of the coast phase.

The heat rates to the ullage prior to venting are shown in figure 24. During this period. the vent valves were closed and the tank pressure instrumentation indicated a pressure rise rate of 0.48 pound per square inch absolute per minute (55 $N/(m^2)$(sec)). The internal tank temperature sensors indicated an average ullage bulk temperature of 42° R (23° K) at the initiation of the coast period. With the heat rates presented, the calculated pressure rise rate and the calculated temperature rise for the period in which the vent valves are closed can be calculated from equation (D3), with M_v and M_b equal to zero and M_i equal to M_f, by solving for U_f. The calculated pressure rise rate is 0.46 pound per square inch per minute (53 $N/(m^2)$(sec)), and the calculated temperature at the time of first venting is 54° R (30° K). The temperature measured by the temperature sensors was also 54° R (30° K). The comparison between the calculated and the measured pressure rise rate, temperature, and vented quantity indicates the accuracy of the thermal surveys performed on the AC-8 mission.

REFERENCES

1. Hastings, G. A.; Hill, D. W.; Satterlee, H. M.; and Seebold, J. G.: The Literature of Low G Propellant Behavior. Rep No. LMSC-A835805 (NASA CR-65539), Lockheed Missiles and Space Co., Sept. 27, 1966.

2. Chipchak, D.; Brady, V.; Warner, P.; Wallace, J.; Fejer, G.; Schmidt, C.; and Vecchies, L.: Development of Expulsion and Orientation Systems for Advanced Liquid Rocket Propulsion Systems. (AFRTD-TDR-63-1048), Bell Aerosystems Co., July 1963.

3. Ring, Elliot: Rocket Propellant and Pressurization Systems. Prentice Hall, Inc., 1964.

4. Szabo, Steven V., Jr.; Groesbeck, William A.; Baud, Kenneth W.; Stofan, Andrew J.; Porada, Theodore W.; and Yeh, Frederick C.: Atlas-Centaur Flight AC-4 Coast-Phase Propellant and Vehicle Behavior. NASA TM X-1189, 1965.

5. Banks, Robert B.; and Chandrasekhara, D. V.: Experimental Investigation of the Penetration of a High-Velocity Gas Jet Through a Liquid Surface. J. Fluid Mech., vol. 15, pt. 1, Jan. 1963, pp. 13-34.

6. Sumner, Irving E.; Stofan, Andrew J.; and Shramo, Daniel J.: Experimental Sloshing Characteristics and a Mechanical Analogy of Liquid Sloshing in a Scale-Model Centaur Liquid Oxygen Tank. NASA TM X-999, 1964.

7. Sumner, Irving E.; Lacovic, Raymond F.; and Stofan, Andrew J.: An Experimental Investigation of Liquid Sloshing in a Scale-Model Centaur Liquid-Hydrogen Tank. NASA TM X-1313, 1966.

8. Staff of the Lewis Research Center: Postflight Evaluation of Atlas-Centaur AC-8 (Launched April 7, 1966). NASA TM X-1343, 1967.

9. Berns, James A.; Yeh, Frederick C.; and Nussle, Ralph C.: Photographic Investigation of Liquid Behavior on Temperature and Liquid-Vapor Sensors Used in Low-Gravity Environment. NASA TM X-1438, 1967.

10. Chelton, Dudley B.; and Mann, Douglas B.: Cryogenic Data Book. (WADC TR 59-8, DDC No. AD-208155), National Bureau of Standards, Cryogenic Eng. Lab., Mar. 1959.

11. Forstall, Walton: and Gaylord, E. W.: Momentum and Mass Transfer in a Submerged Water Jet. J. Appl. Mech., vol. 77, no. 2, June 1955, pp. 161-164.

Nose fairing

Surveyor mass model

Centaur liquid hydrogen tank

Centaur liquid oxygen tank

Insulation panels

Interstage adapter

Intermediate bulkhead

Centaur main engines

Atlas oxidizer tank

Atlas fuel tank

Atlas main engines
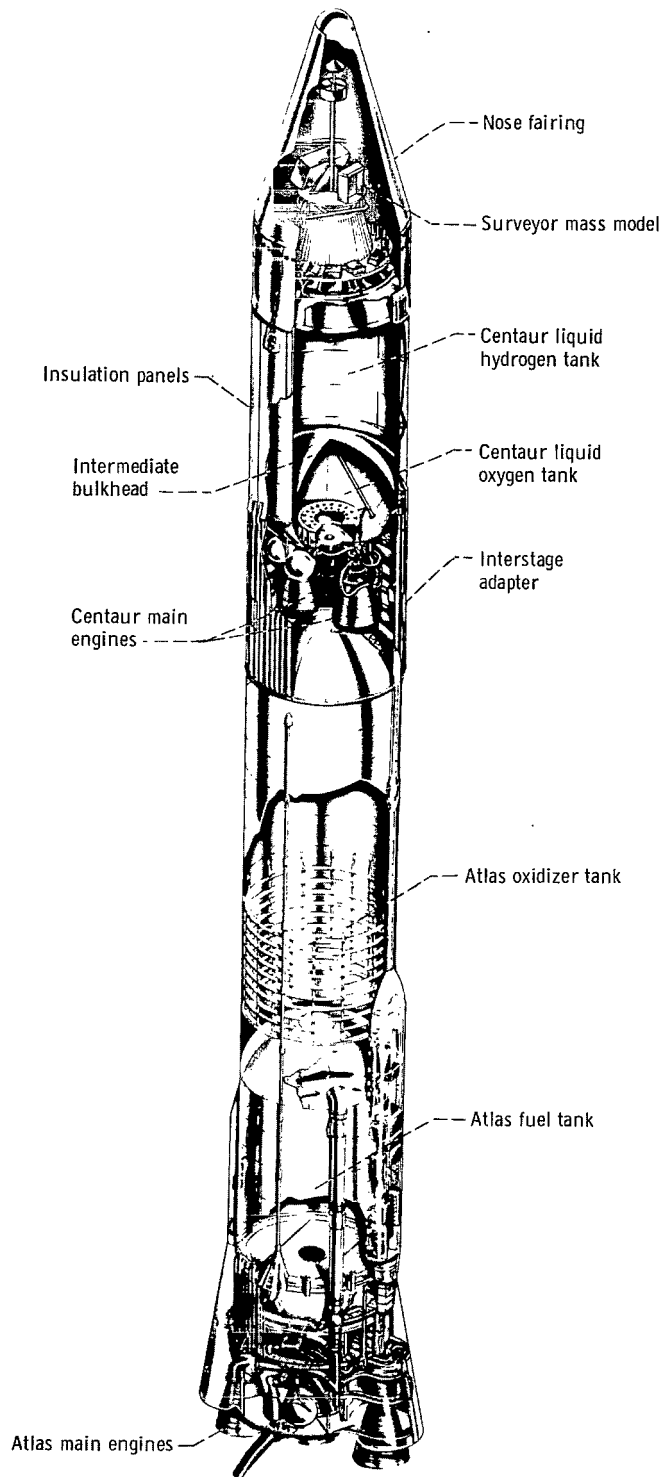
CD-9228

Figure 1. - Atlas-Centaur-Surveyor configuration.

33

Centaur
second burn

Propellant
retention

First Centaur
main engine
cutoff (T + 578 sec)

Spacecraft
separation

First Centaur
main engine
start (T + 240 sec)

Centaur
first burn

Spacecraft

First Centaur
main engine
start (T + 240 sec)

Second main
engine start
(T + 2030 sec)

Centaur turn around and retromaneuver

Atlas-Centaur
separation phase

Propellant
settling
(100 sec)

Propellant
suppression
(46 sec)

Centaur
mission
complete

Jettison nose fair-
ing (T + 204 sec)

Jettison insula-
tion panels (T + 177 sec)

Atlas
sustainer
phase

Booster engine cut-
off (T + 143 sec)

Atlas
booster
phase

CD-9414

Liftoff (T = 0 sec)

Figure 2. - Centaur two-burn flight sequence.
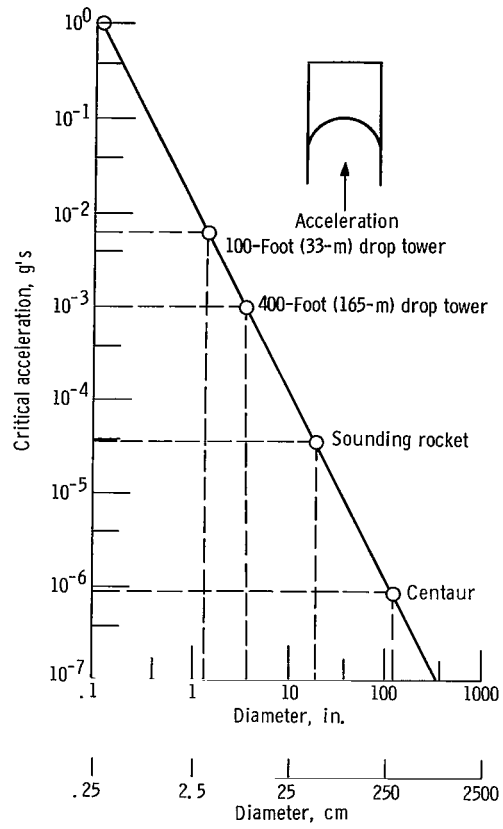
Figure 3. – Minimum acceleration requirements
as function of tank diameter.
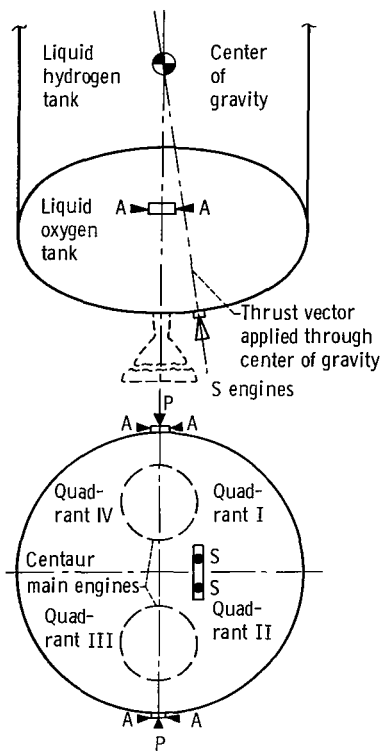
Engine	Thrust		Function
designation	lb	N	
A	1.5	6.5	Attitude control
P	3	13	Attitude control
S	2	9	Propellant settling

Figure 4. - Location of AC-4 attitude control
and propellant settling engines.
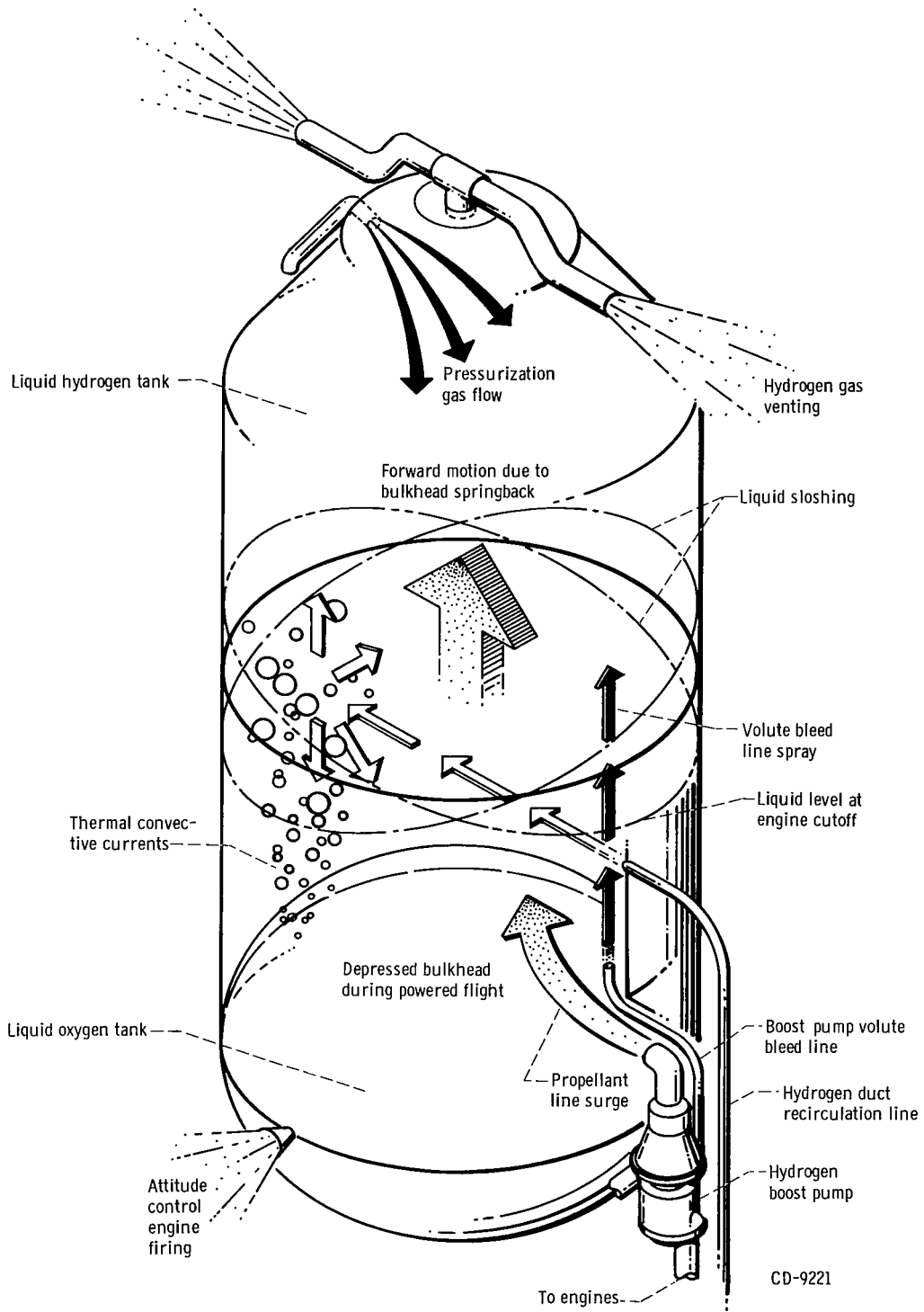
Figure 5. - Energy inputs to AC-4 liquid hydrogen tank.

The labels in the figure read:

Liquid hydrogen tank

Pressurization gas flow

Hydrogen gas venting

Forward motion due to bulkhead springback

Liquid sloshing

Thermal convective currents

Volute bleed line spray

Liquid level at engine cutoff

Depressed bulkhead during powered flight

Liquid oxygen tank

Propellant line surge

Attitude control engine firing

Boost pump volute bleed line

Hydrogen duct recirculation line

Hydrogen boost pump

To engines

CD-9221

Figure 6. – AC-4 Centaur liquid hydrogen supply system.
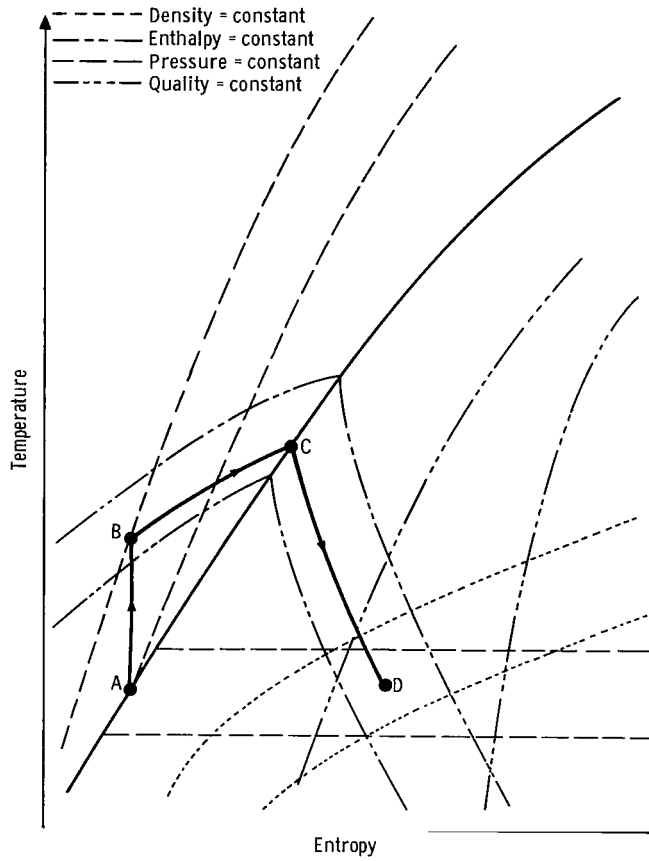
Figure 7. – Energy dissipation process on temperature-entropy diagram.

Lower edge of liquid
hydrogen tank baffle

Liquid hydrogen
recirculation line
energy dissipator

Boost pump volute
bleed energy
dissipator

C-67-3268
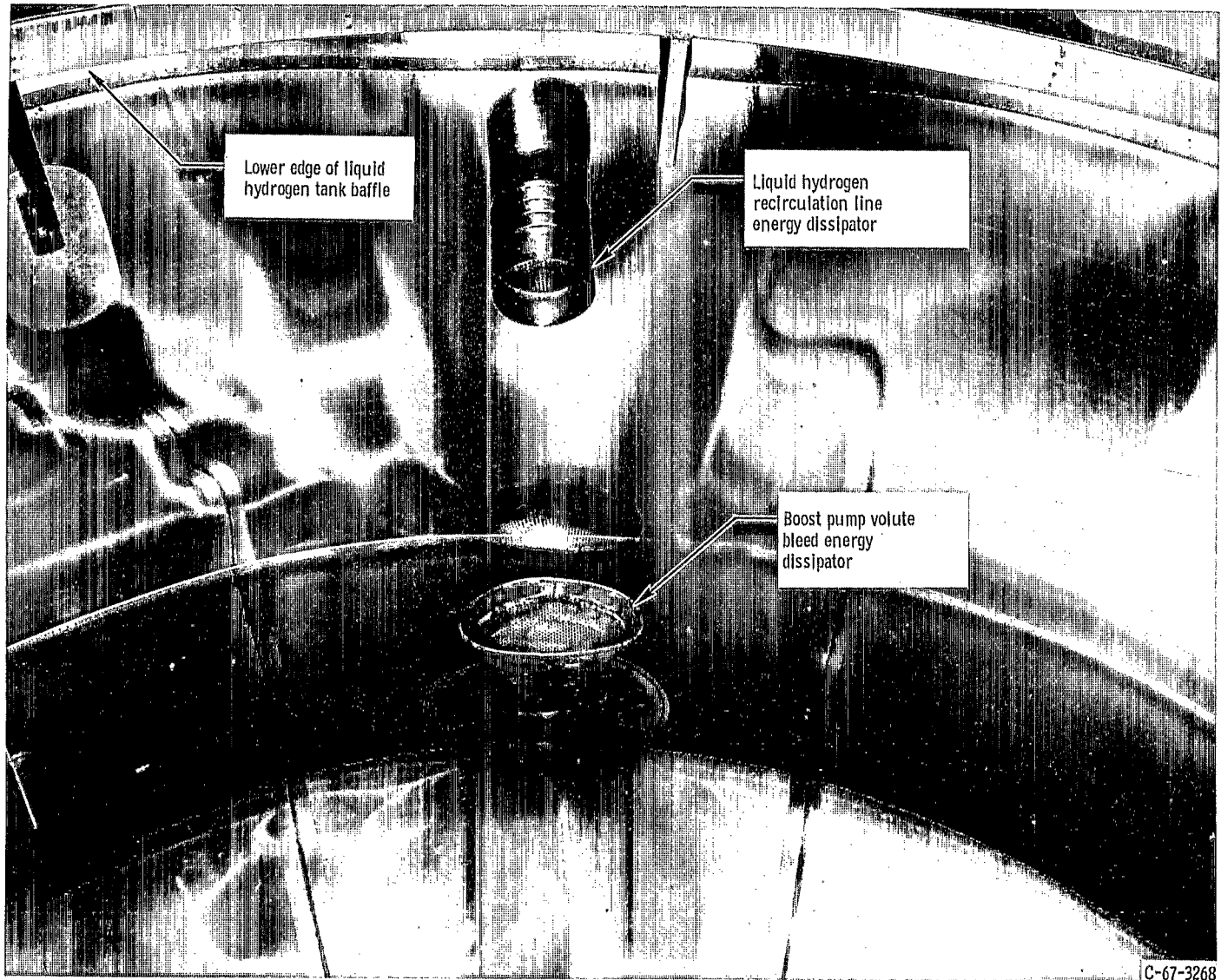
(a) Volute bleed and recirculation line energy dissipator as installed in AC-8 liquid hydrogen tank.

Figure 8. - Volute bleed and recirculation line energy dissipators.

Liquid hydrogen tank

Vehicle centerline

1-Inch-diameter (2.5×10^{-2}-m-diam.) tube

Hydrogen duct recircula-tion line energy dissipator

Boost pump volute bleed line energy dissipator

Flow

Intermediate bulkhead

2-Inch-diameter (5.0×10^{-2}-m-diam.) tube

Liquid oxygen tank

Liquid hydrogen boost pump
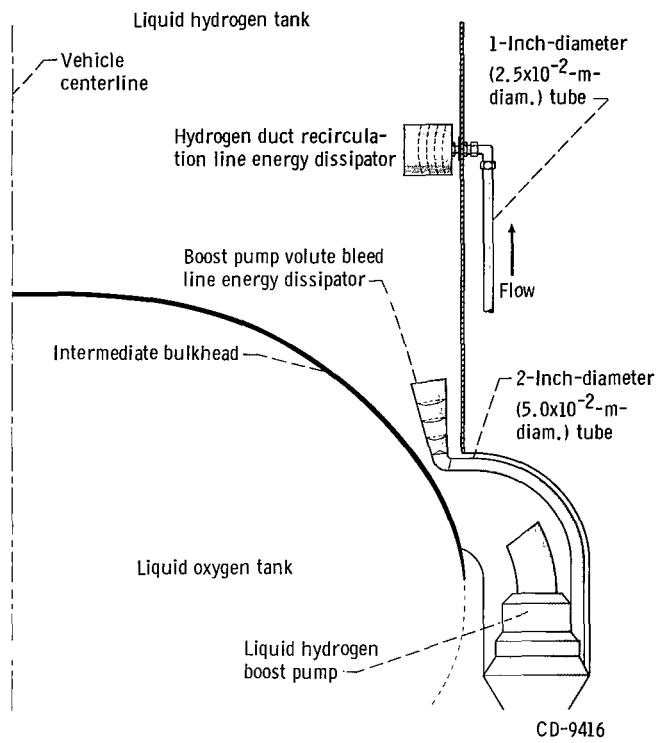
CD-9416

(b) Installation details of volute and recirculation line flow energy dissipator; AC-8.

Figure 8. - Continued.
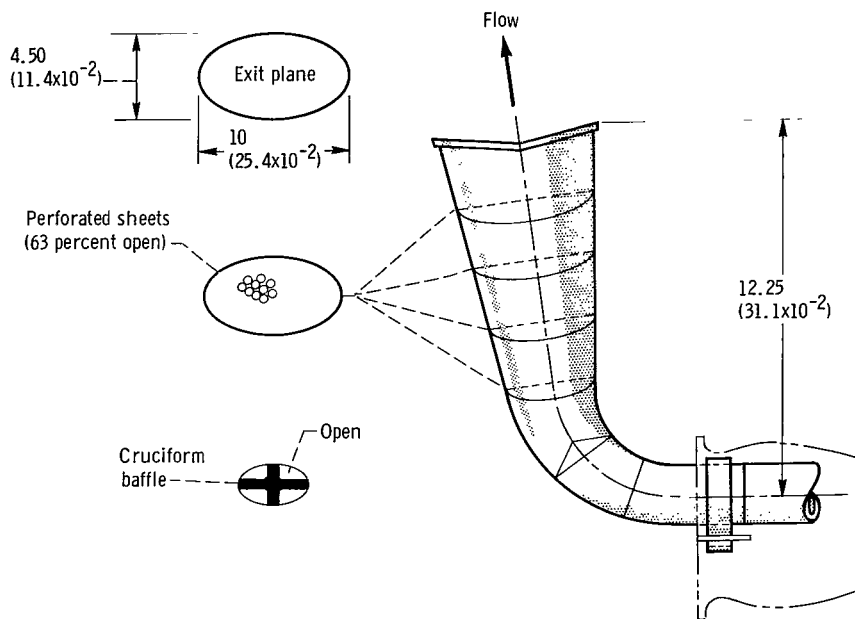
(c) Design details of volute bleed energy dissipator. (All dimensions in inches (meters).)
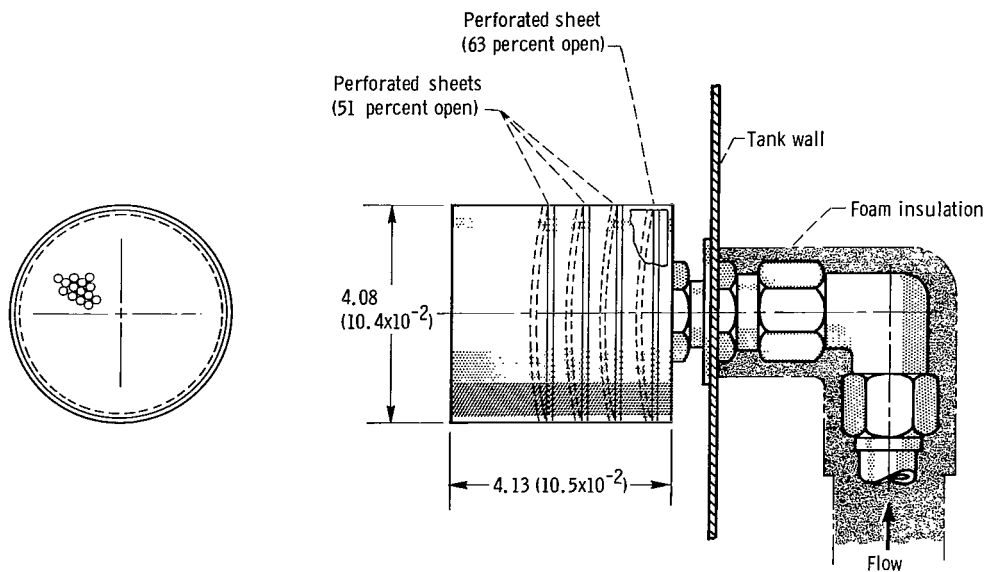
CD-9417

(d) Design details of recirculation line energy dissipator. (All dimensions in inches (meters).)

Figure 8. – Concluded.
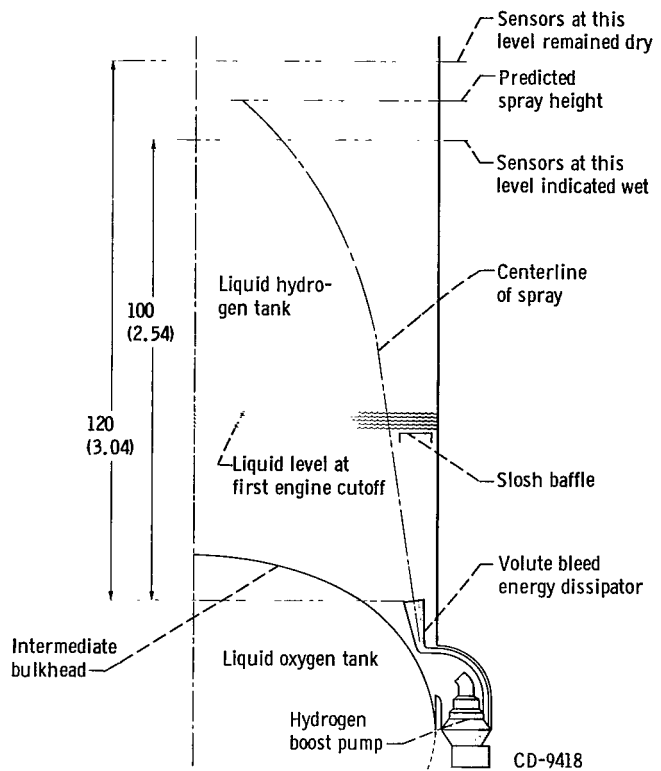
Figure 9. – Predicted spray height for volute bleed spray at first engine cutoff and flight data; AC-8. (All dimensions in inches (meters).)
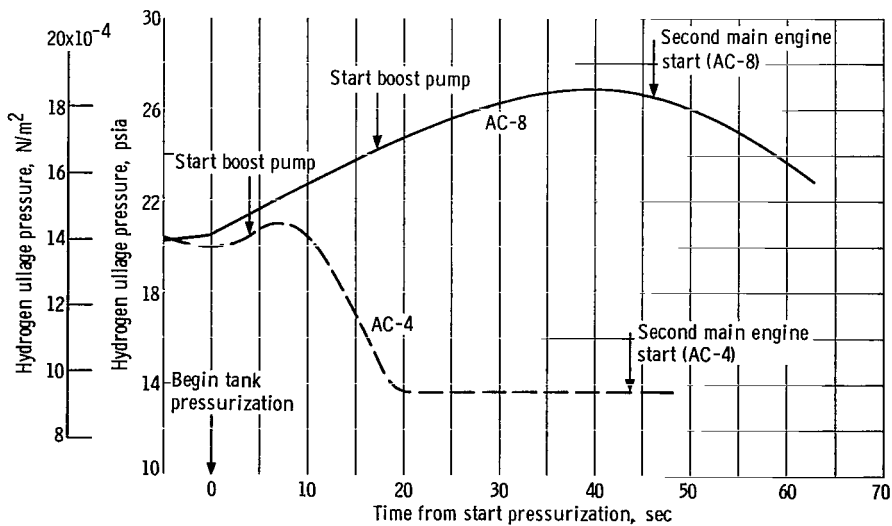
Figure 10. – AC-4 and AC-8 hydrogen tank pressures at second engine start.

Station 179 — Gas flow (high velocity) Station 162

Deflector plate

Hydrogen tank

Liquid level at second engine start station 330

(a) AC-4.

Top of hydro-
gen tank ┌ Plenum

Dissipator

Forward

Centerline
of vehicle

Screens formed
to spherical radius

Screens

Helium

Splitter

Screens

Cone

Liquid hydrogen

Liquid oxygen

30°
(0.524 rad)

10.5 in. (0.267 m)

(b) AC-8.

CD-9419
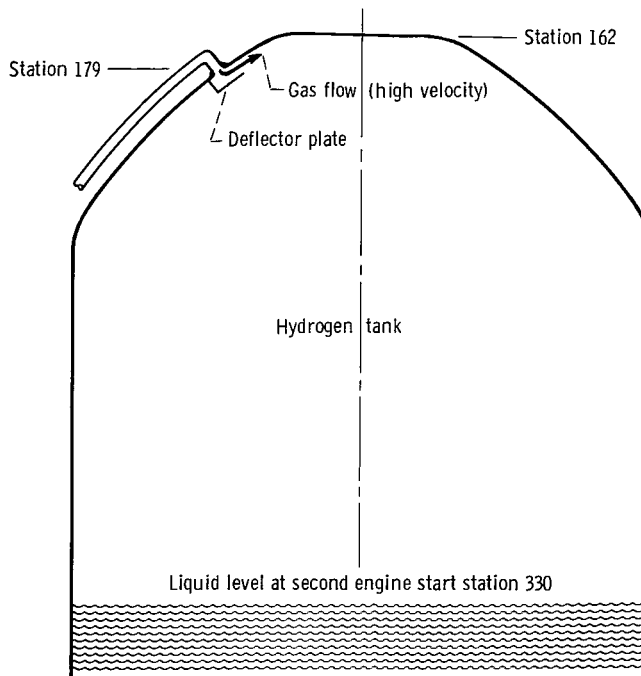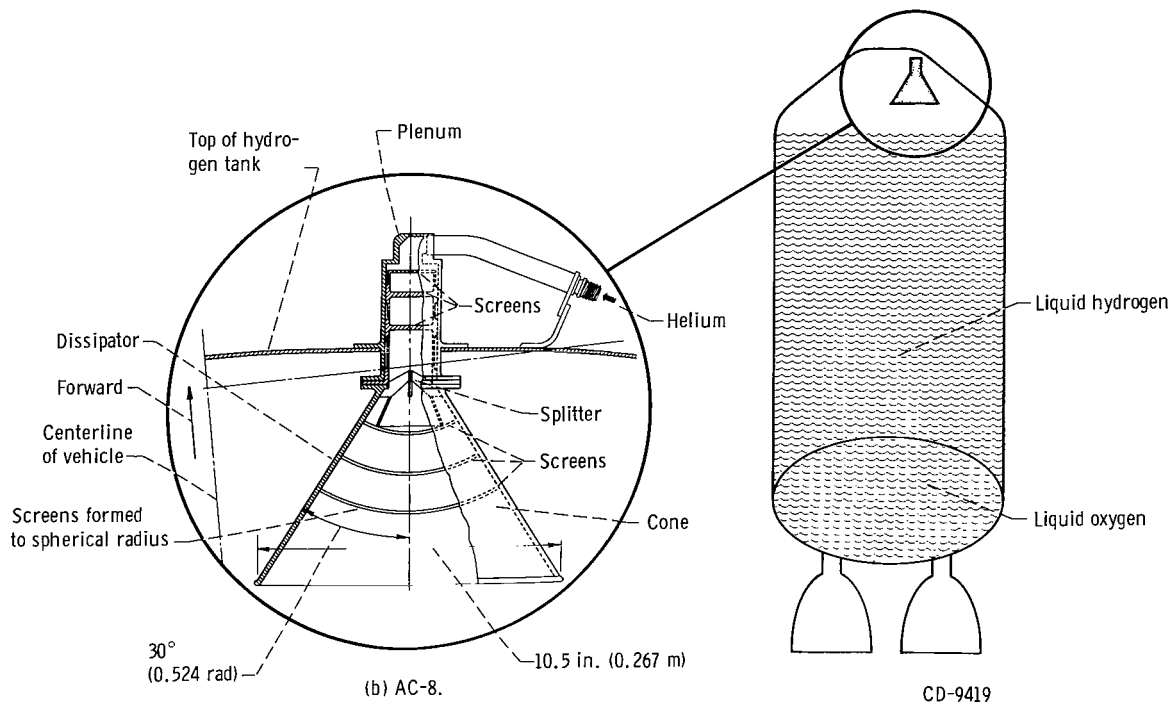
Figure 11. – Hydrogen tank helium pressurization configuration.

44
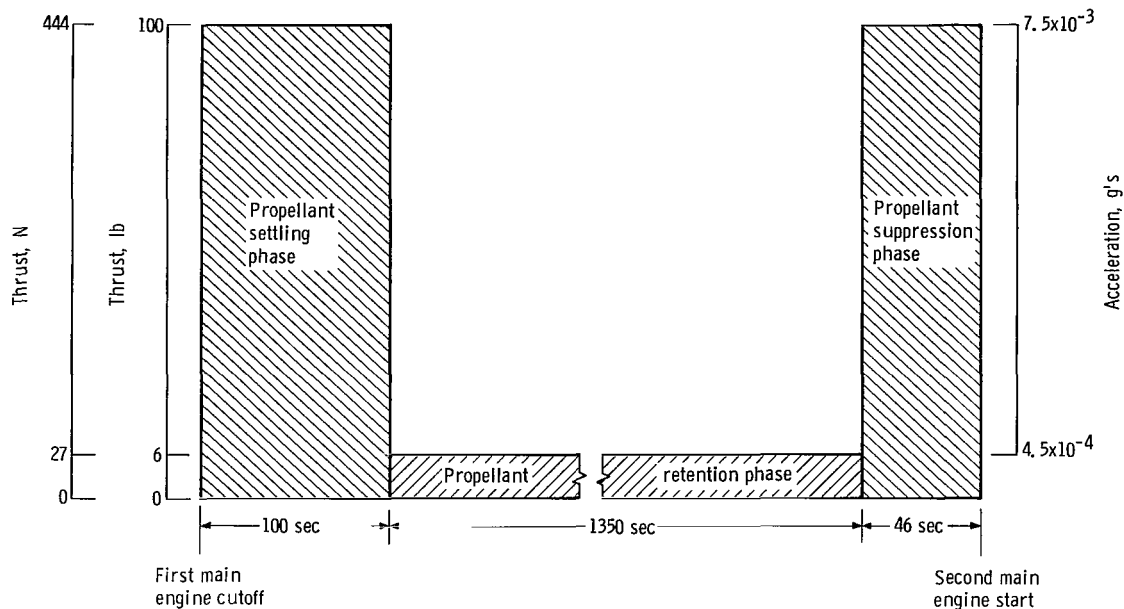
Figure 12. – AC-8 coast phase thrust schedule.

View looking forward
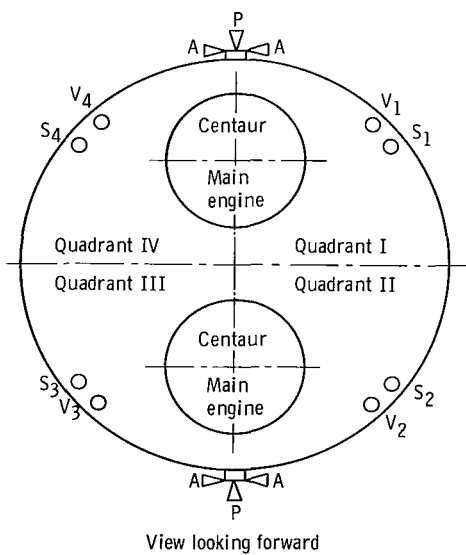
Engine designation	Thrust		Function
	lb	N	
A	3.5	15	Attitude control
V	50	220	Propellant settling, attitude control, and retromaneuver
P	6	27	Attitude control
S	3	13	Propellant retention and attitude control

Figure 13. – Location of AC-8 attitude control and propellant settling engines.

Forward

Vertical antiswirl baffle

Liquid hydrogen tank baffle

C-67-3269
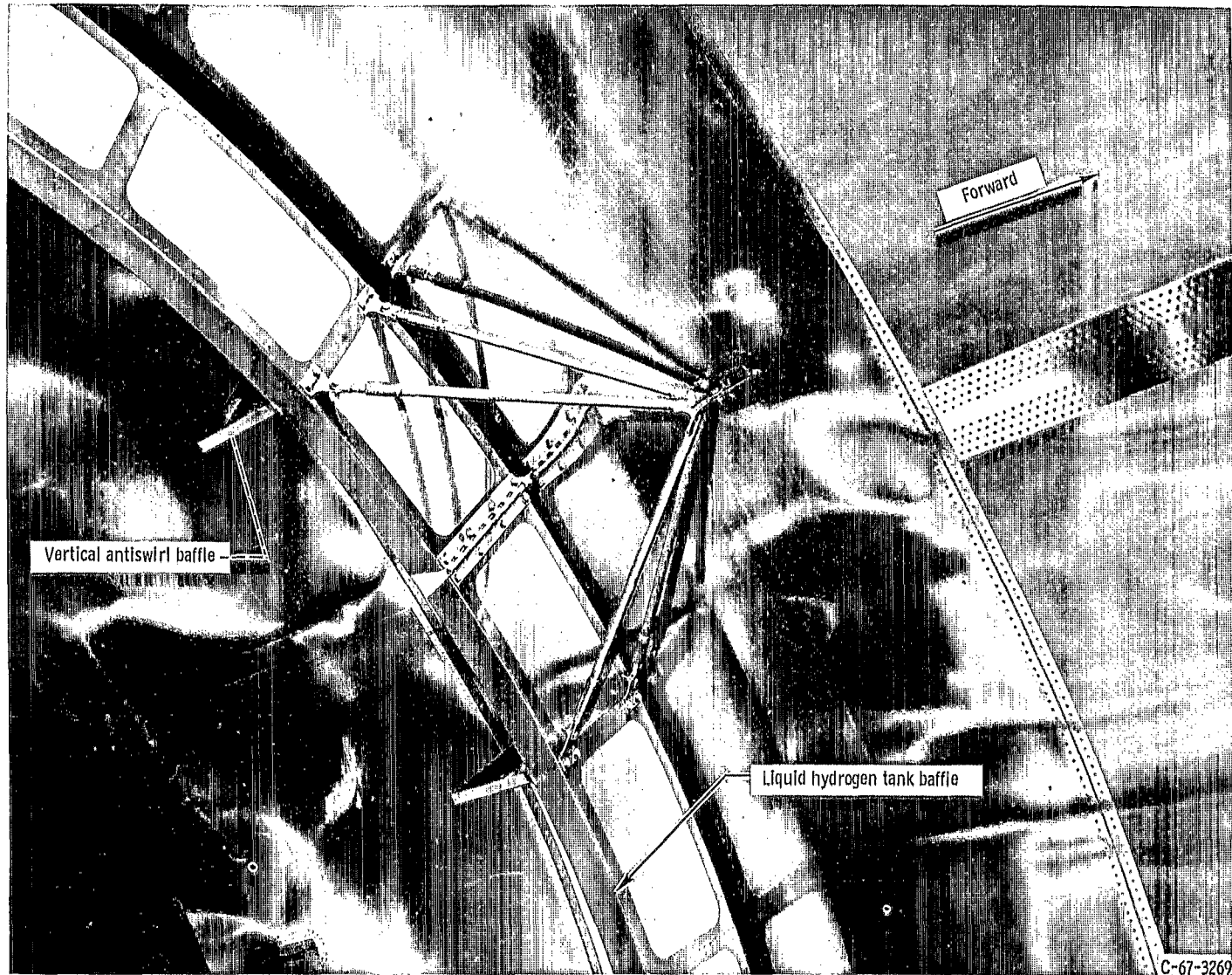
(a) Installed in AC-8 liquid hydrogen tank.

Figure 14. - AC-8 liquid hydrogen slosh baffle.

Typical baffle stiffeners, S

Typical antiswirl baffle, B

1.97 (0.049)
7.95 (0.20)
S_1
7.95 (0.20)
S_2
7.5 (0.19)

Holes (1 in. diam. (0.026 m diam.))

7.95 (0.20)
2 (0.051)

0.50 (0.013)
0.75 (0.019)

Tank wall

Lower baffle support (3 places)

Top-mounted baffle support struts

Antislosh baffle at depth ratio of 0.63

Tank wall
6.7 (0.17)
0.5 (0.013)
16 (0.41)

Lower baffle support

Ratio of distance from tank bottom to diameter (depth ratio), H/D
0.63
.36 (Top of dome)
0

CD-8643

(b) Slosh baffle details and dimensions. (All dimensions in inches (meters).)

Figure 14. – Concluded.
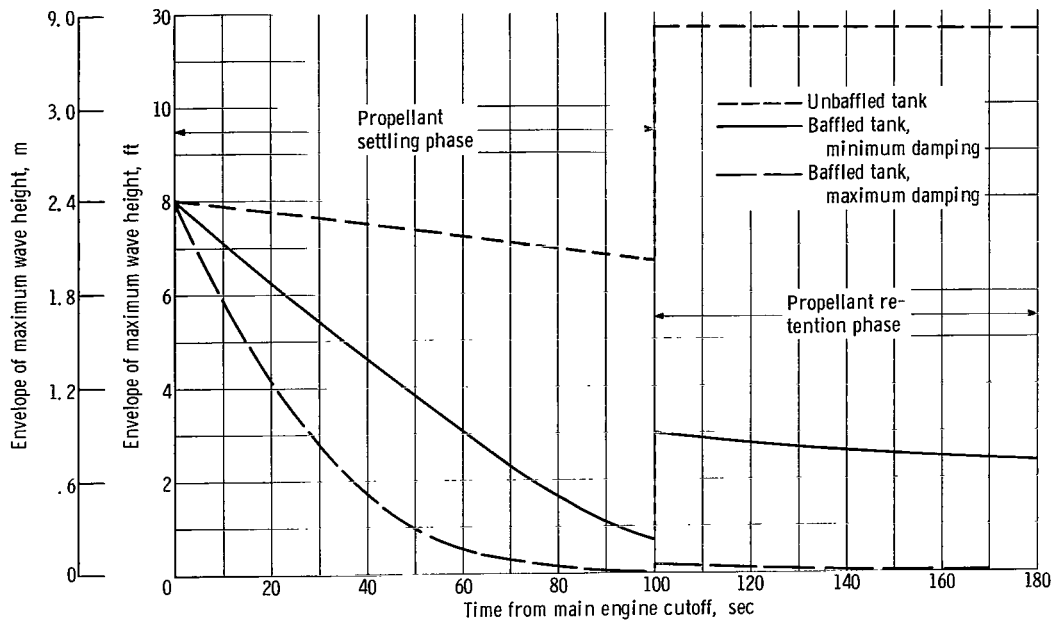
Figure 15. - Comparison of baffled and unbaffled hydrogen tank damping extrapolated from scale-model data (ref. 7).
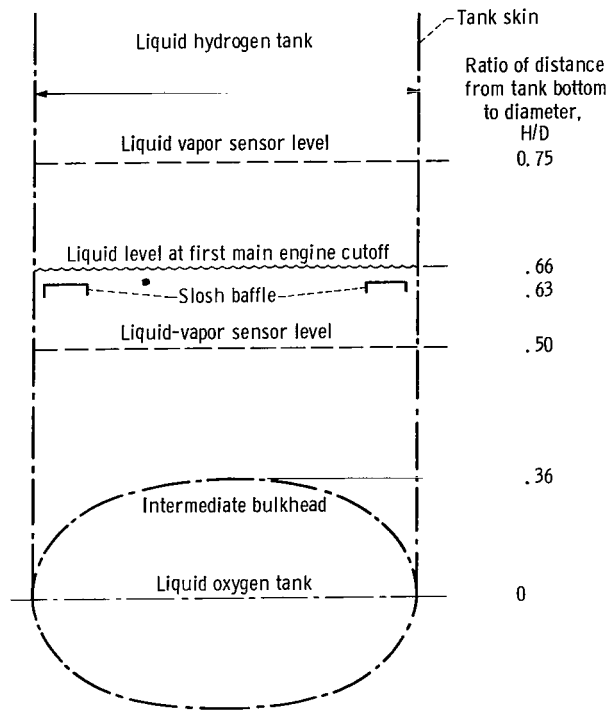
Figure 16. - Schematic of liquid hydrogen tank during coast; AC-8.

Aft view
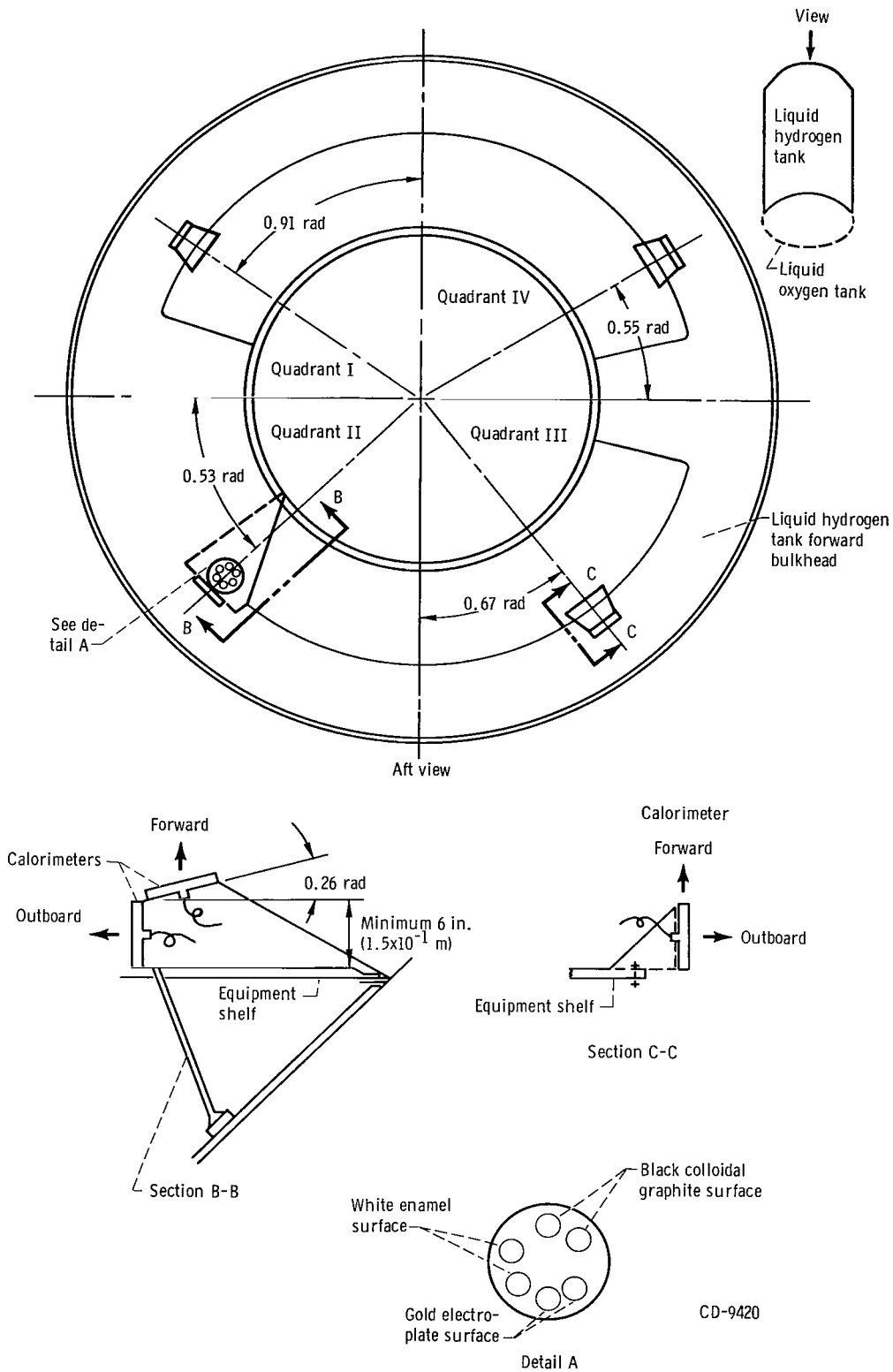
Figure 17. – AC-8 calorimeter locations.
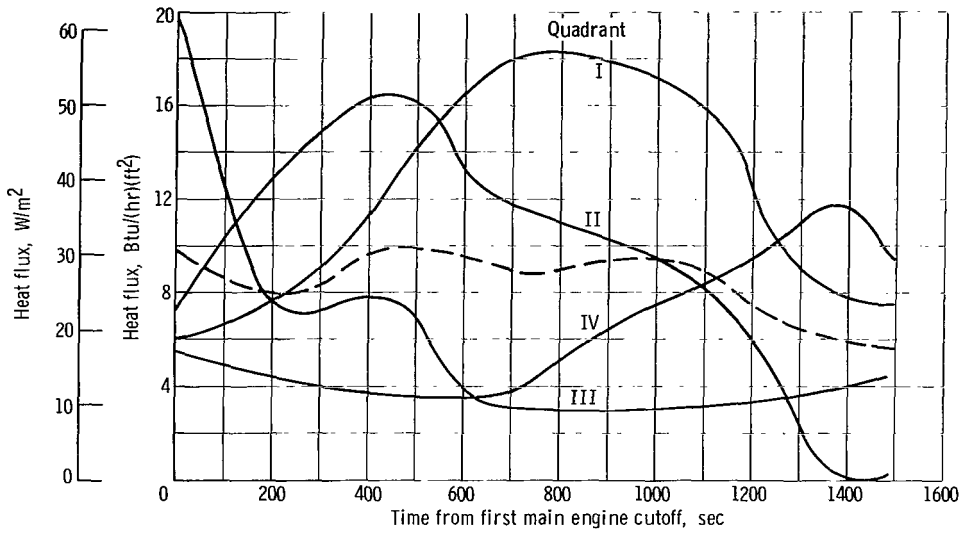
Figure 18. – Environmental heat flux to Centaur liquid hydrogen tank side wall.
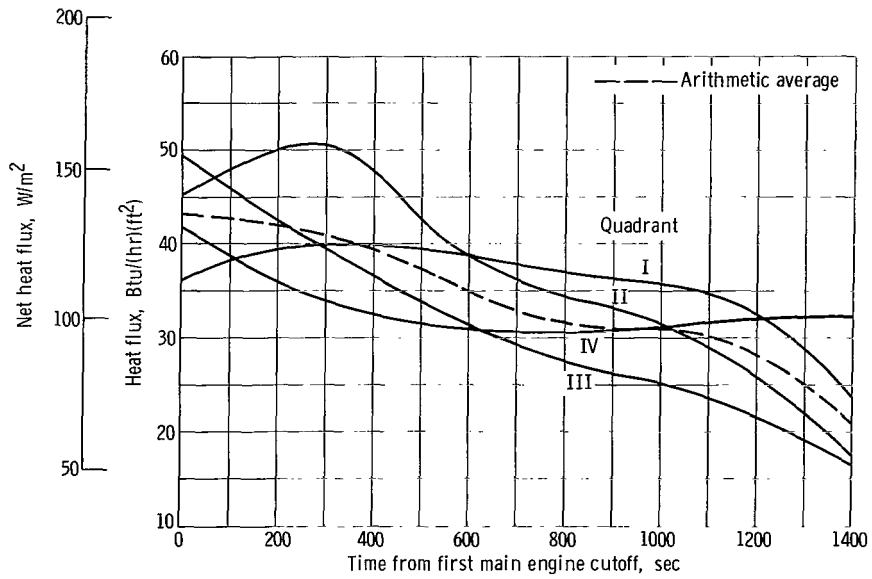
Figure 19. – Environmental heat flux into forward end of Centaur hydrogen tank.
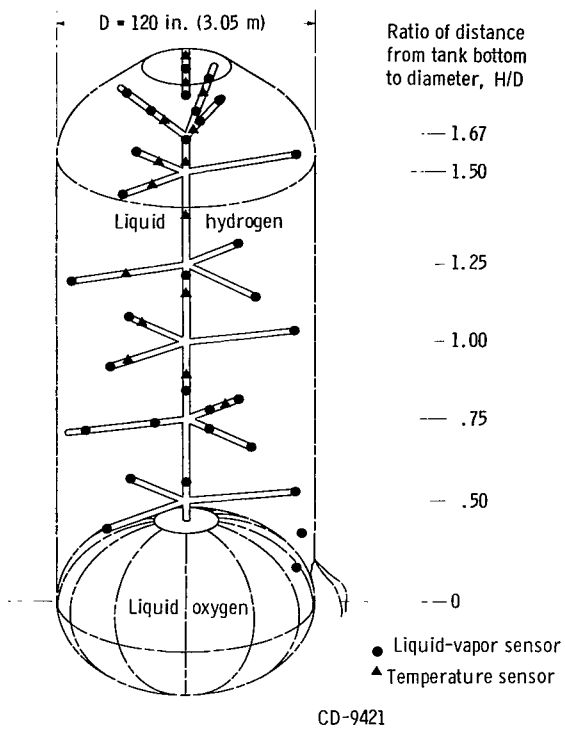
Figure 20. - Liquid-vapor and ullage gas temperature instrumentation; AC-8.
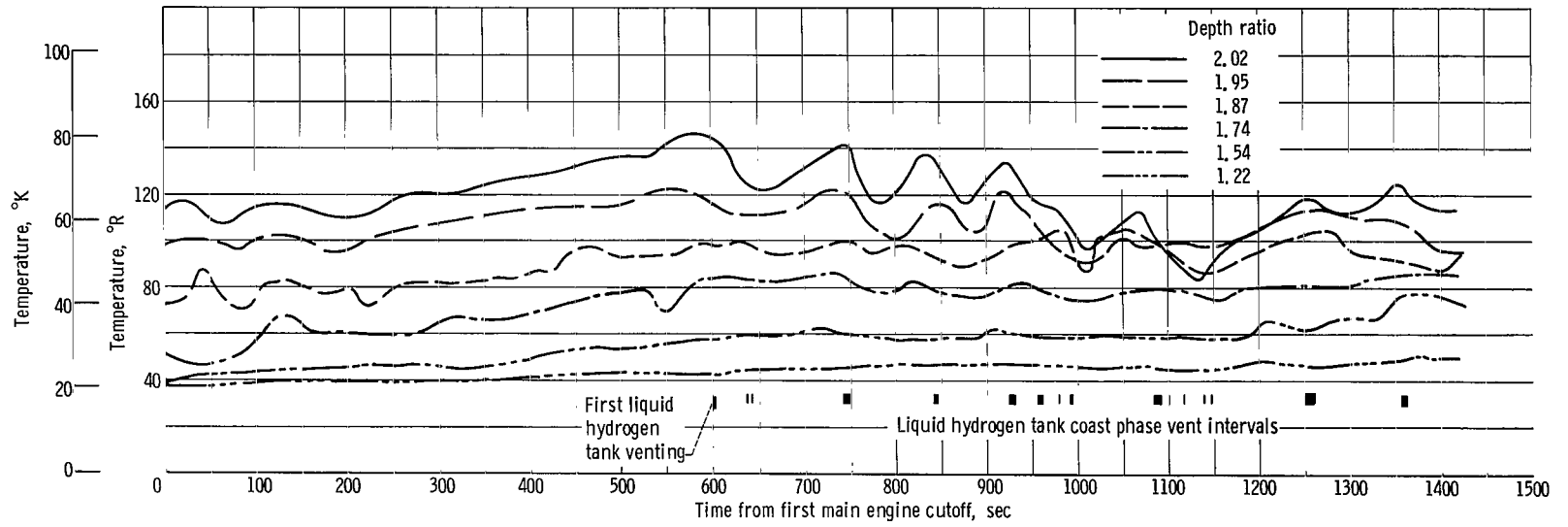
Figure 21. – Liquid hydrogen tank ullage temperature profile.

Quadrant II—
—Quadrant IV
Forward area—
Quadrant III
Tank skin temperature sensors—
10 in. (0.25 m)
Tank skin temperature sensors—
—Centaur main engines

(a) Front view.

Quadrant IV—
—Quadrant II
Quadrant I
—Tank skin temperature sensors—
10 in. (0.25 m)
—Tank skin temperature sensors
—H/D = 0.47
—Liquid hydrogen boost pump
—Liquid oxygen boost pump
CD-9222

(b) Back view.
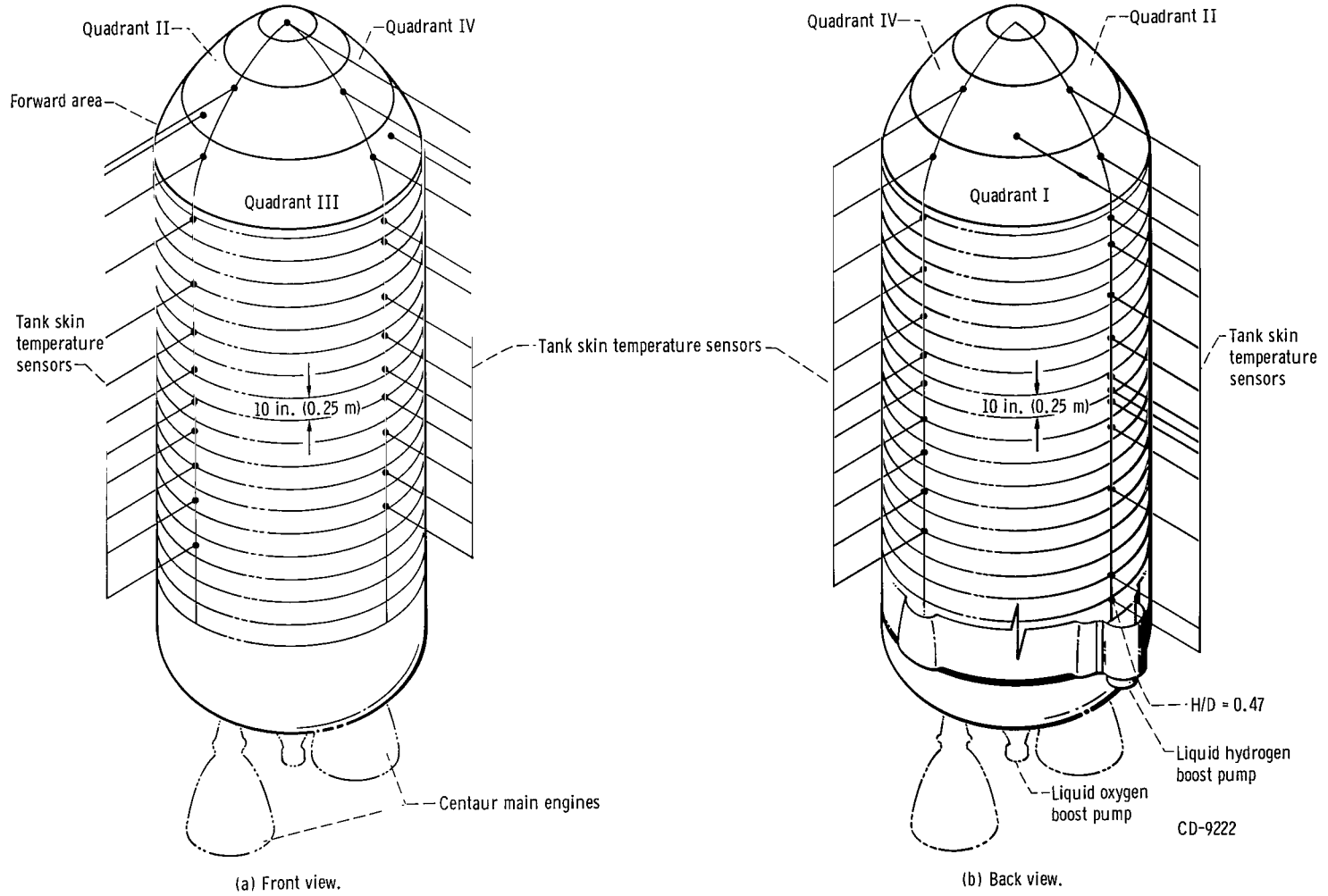
Figure 22. – Centaur tank skin temperature instrumentation. View (b) rotated 180° from view (a).
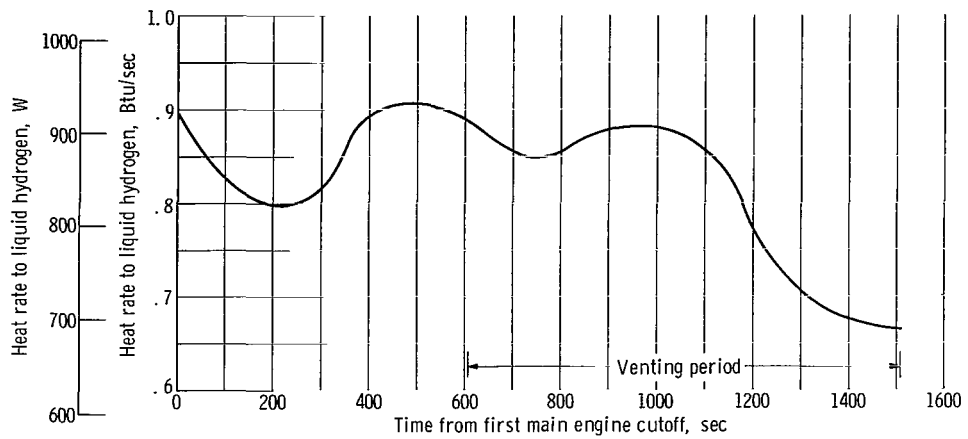
Figure 23. - Heat rate to Centaur liquid hydrogen during coast.
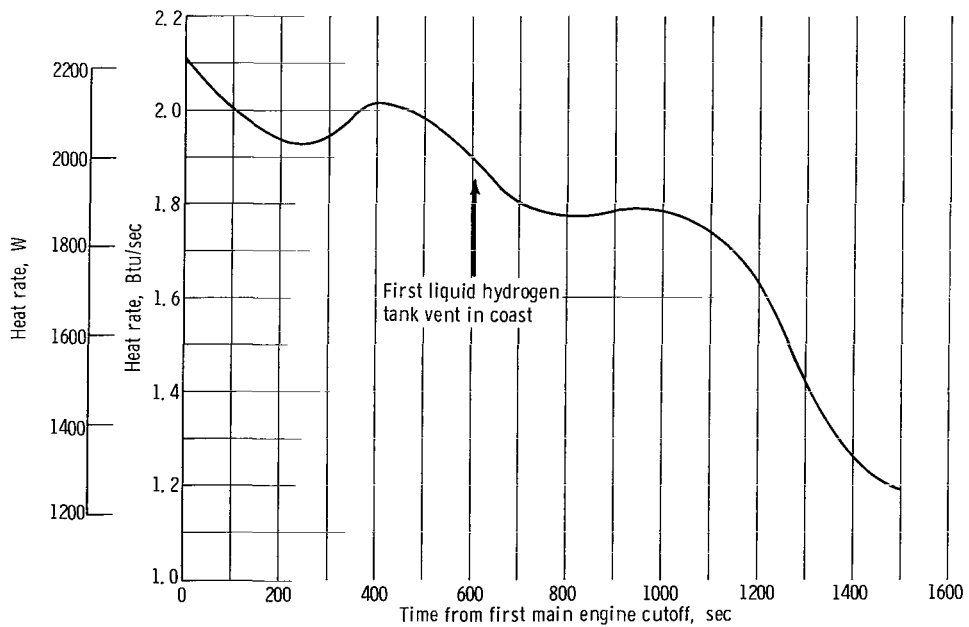
Figure 24. - Heat rate to liquid hydrogen tank ullage.
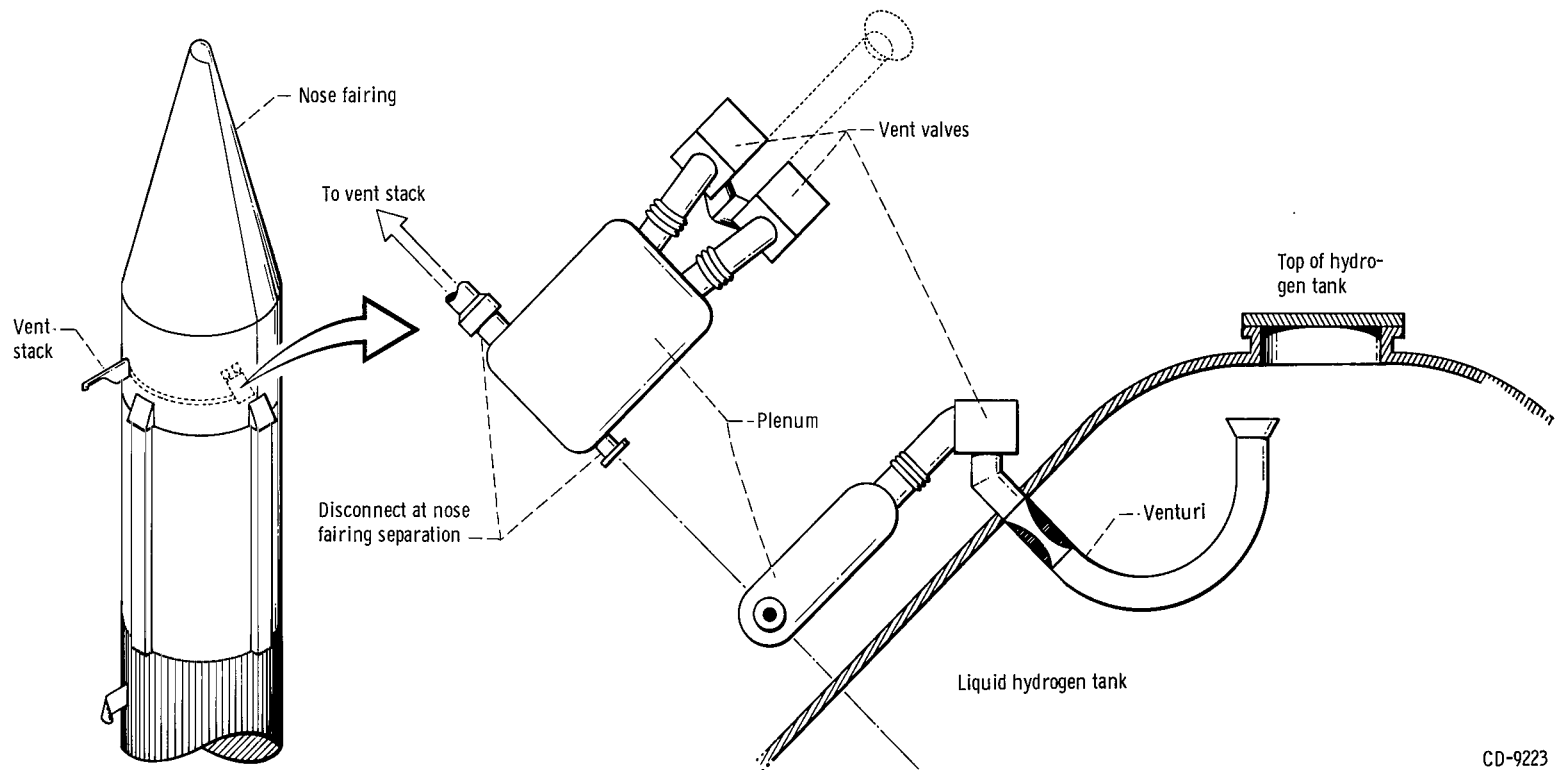
Figure 25. - AC-4 coast phase hydrogen vent system.

- Nose fairing

To vent stack

Vent valves

Top of hydro-
gen tank

Vent
stack

Plenum

Disconnect at nose
fairing separation

Venturi

Liquid hydrogen tank

CD-9223

Payload adapter

Vent valve 1

Torus assembly

Equipment shelf

Nozzle

Forward bulkhead of hydrogen tank

Vent valve 2
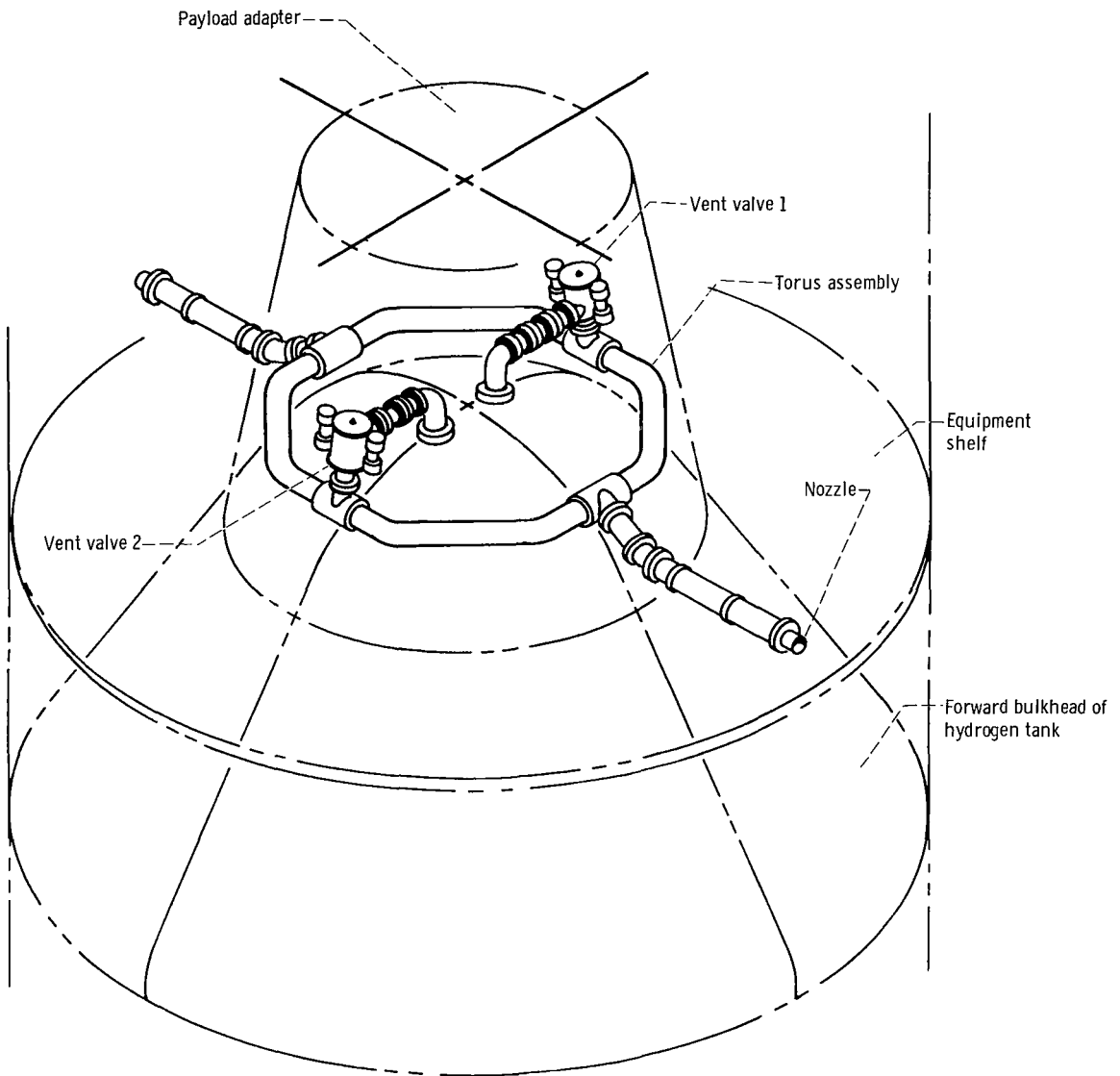
Figure 26. - AC-8 balanced thrust hydrogen vent system.
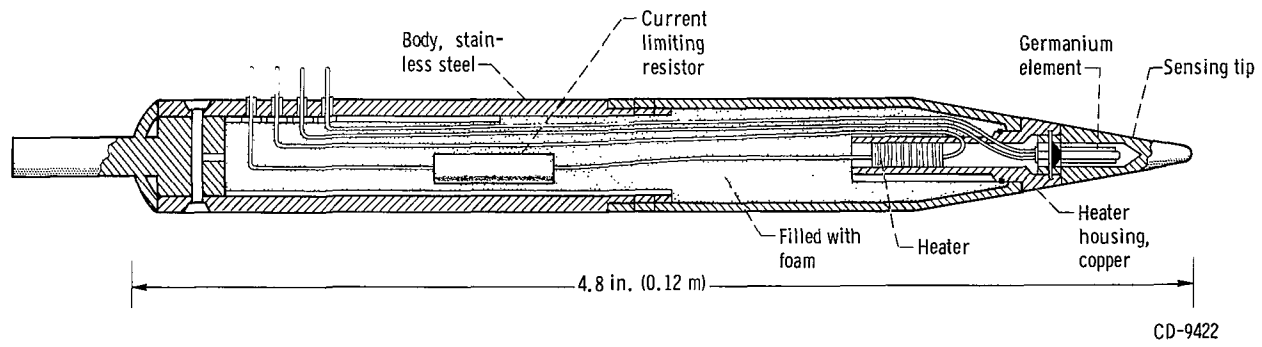
Figure 27. - Liquid-vapor sensor assembly.
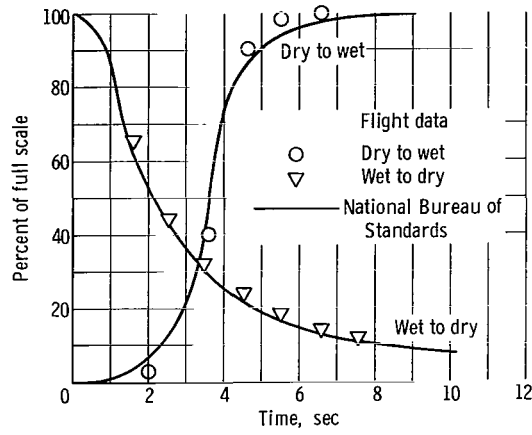
Figure 28. - Liquid-vapor sensor response.
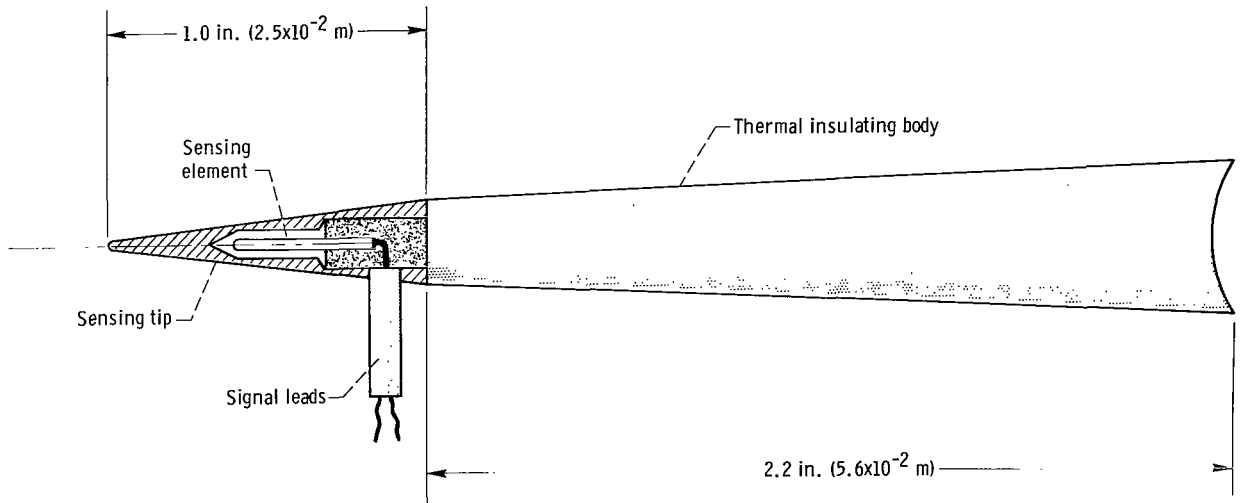
CD-9423

Figure 29. - Ullage temperature sensor assembly.

58
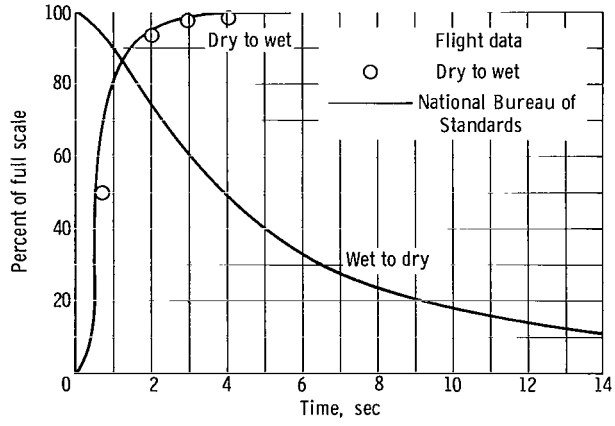
Figure 30. – Ullage temperature sensor response (platinum).
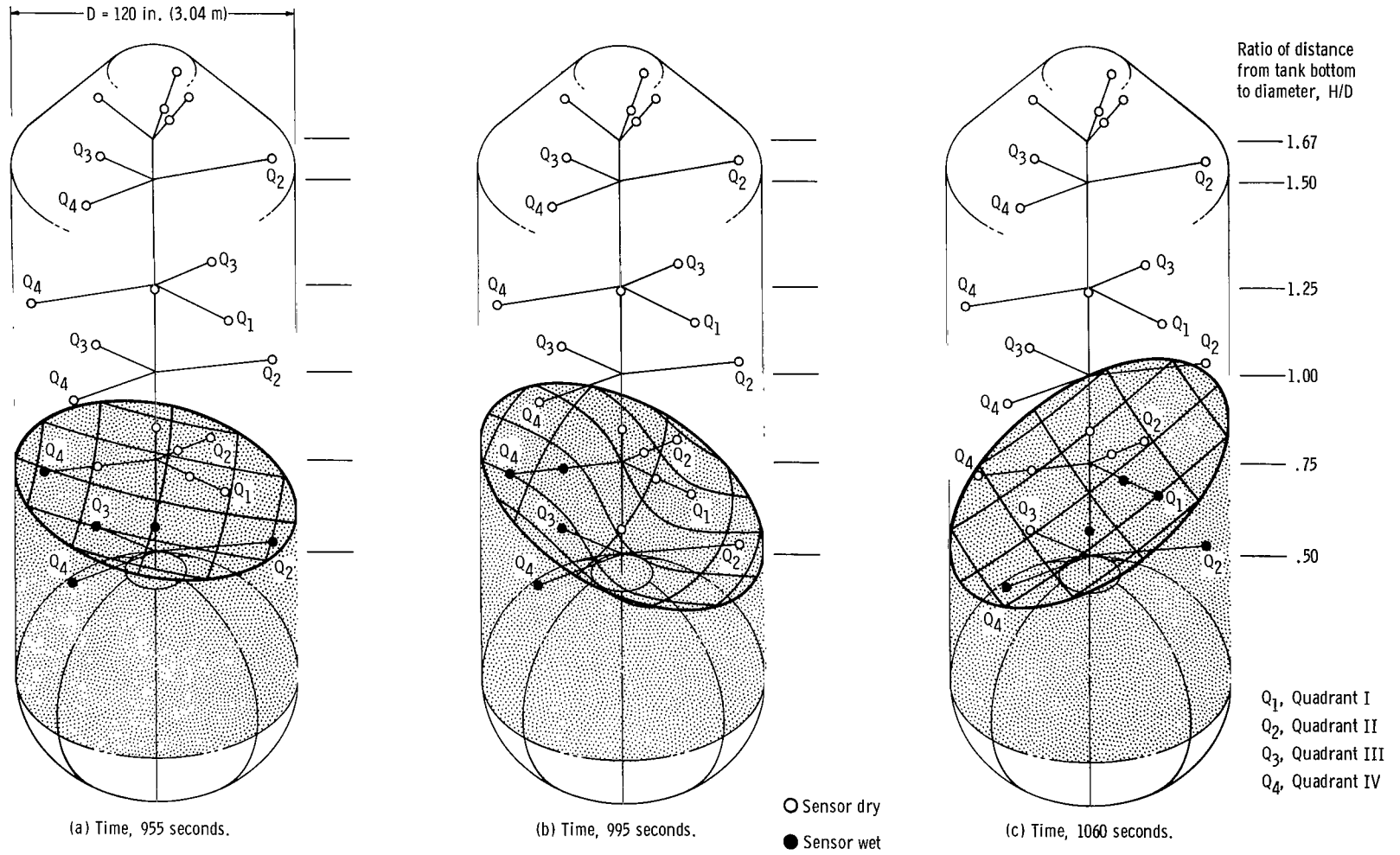
Figure 31. – AC-8 propellant sloshing during propellant retention period. First slosh wave 919 to 1062 seconds after first main engine cutoff.

D = 120 in. (3.04 m)

Ratio of distance from tank bottom to diameter, H/D

—1.67
—1.50
—1.25
—1.00
—.75
—.50

Q_1, Quadrant I
Q_2, Quadrant II
Q_3, Quadrant III
Q_4, Quadrant IV

○ Sensor dry
● Sensor wet

(a) Time, 1075 seconds.

(b) Time, 1098 seconds.

(c) Time, 1192 seconds.
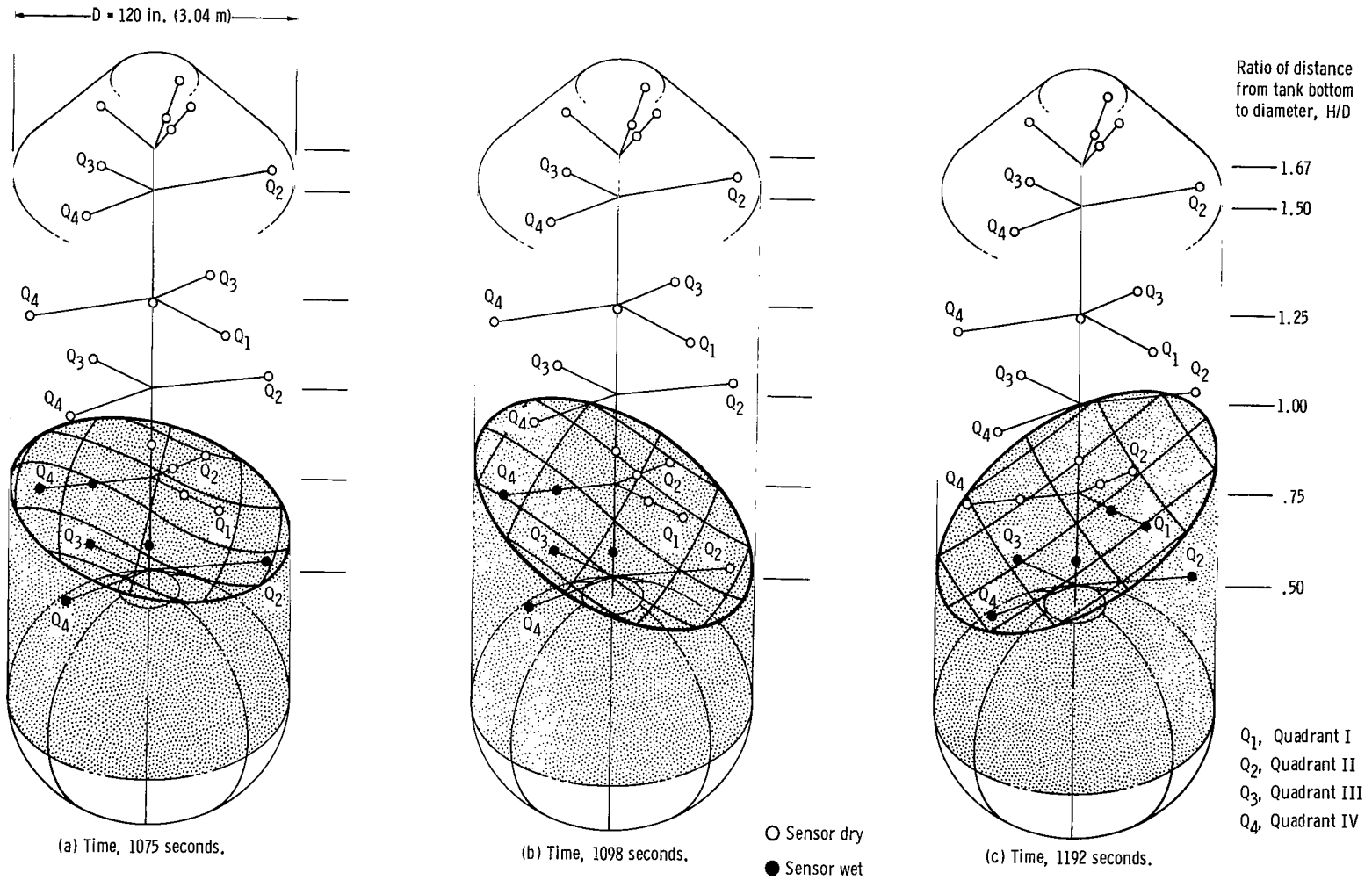
CD-9225

Figure 32. – Second slosh wave 1063 to 1192 seconds after first main engine cutoff.
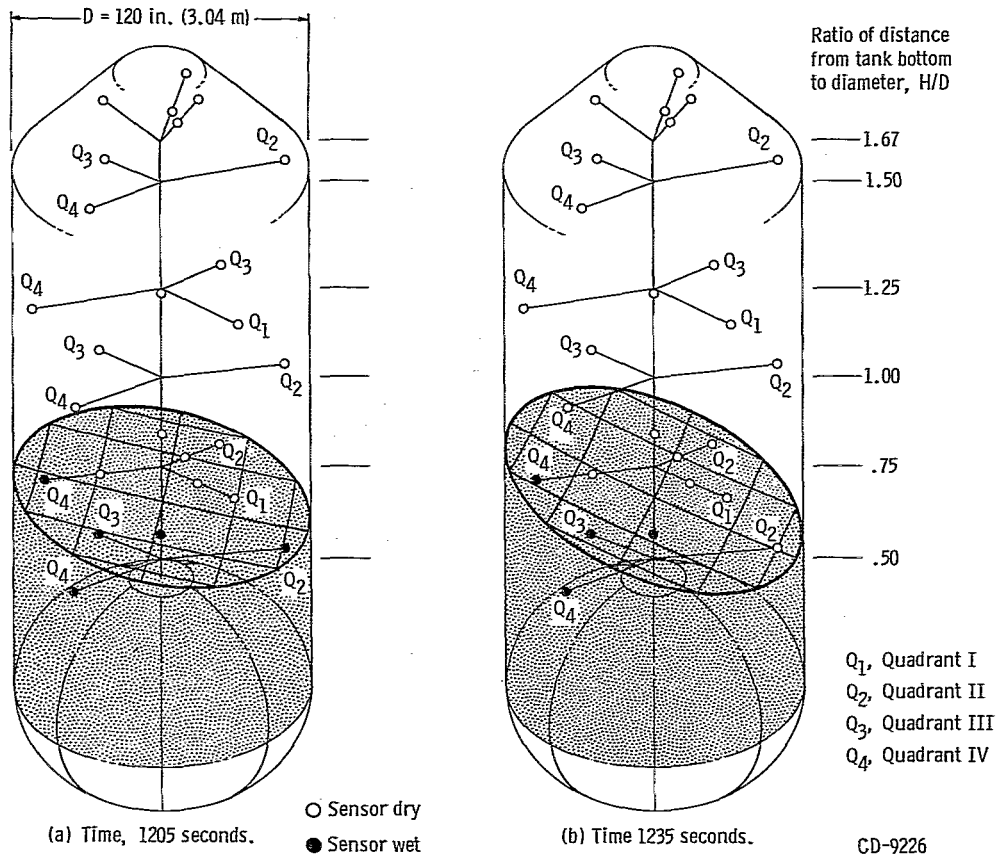
Figure 33. – Third slosh wave 1193 to 1315 seconds after first main engine cutoff.
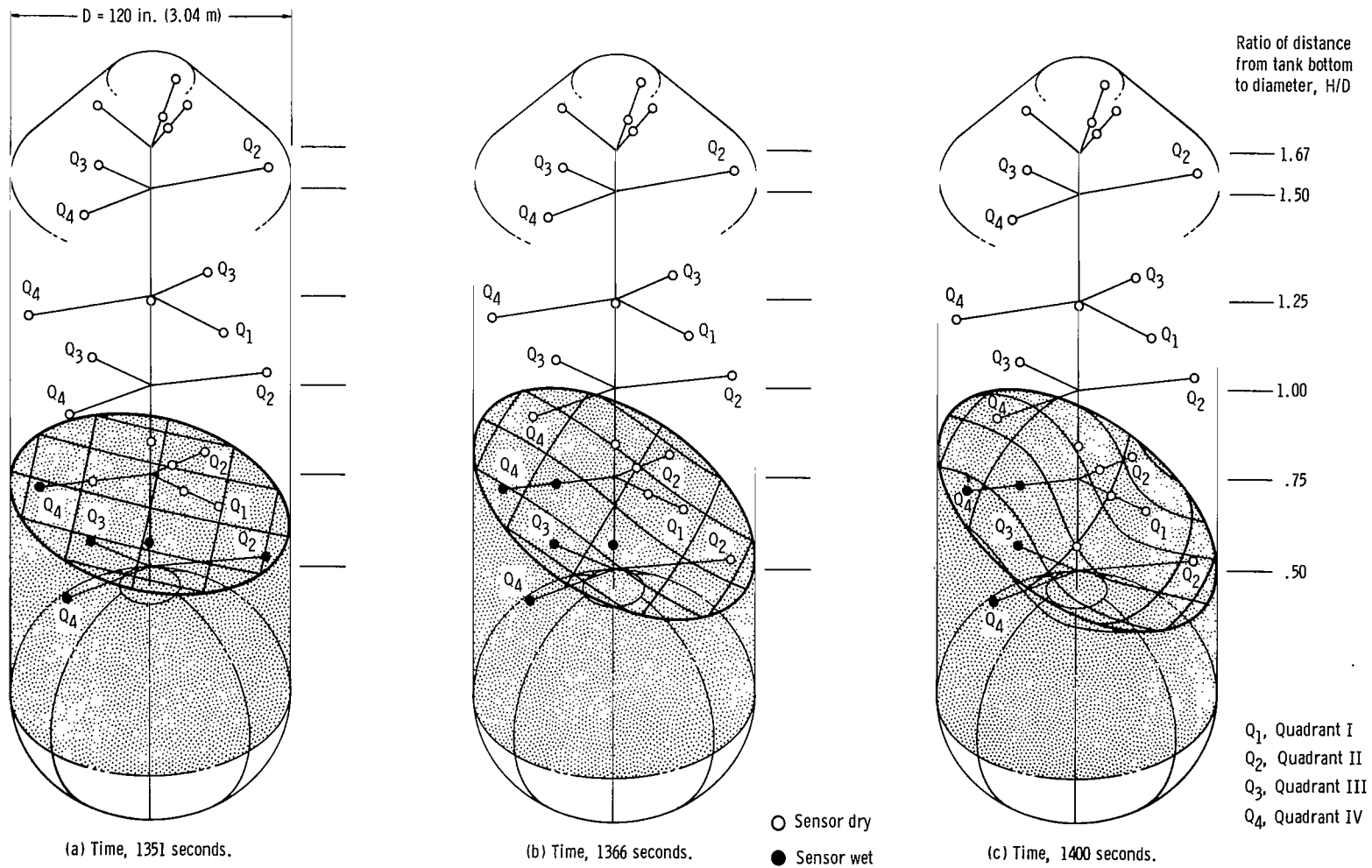
Figure 34. - Fourth slosh wave 1316 to 1449 seconds after first main engine cutoff.

D = 120 in. (3.04 m)

Ratio of distance from tank bottom to diameter, H/D

1.67
1.50
1.25
1.00
.75
.50

(a) Time, 1351 seconds.

(b) Time, 1366 seconds.

(c) Time, 1400 seconds.

○ Sensor dry
● Sensor wet

Q₁, Quadrant I
Q₂, Quadrant II
Q₃, Quadrant III
Q₄, Quadrant IV

CD-9227

Forward view of first two sensor arms

50-Pound (222-N) thrust engine firing data (V_2 and V_3 did not fire during this period)

Liquid-vapor sensor data (solid areas indicate presence of liquid)

Figure 35. – AC-8 liquid-vapor sensor locations and coast phase data.

Figure 36. – Axial acceleration of Centaur during propellant retention period for AC-8.
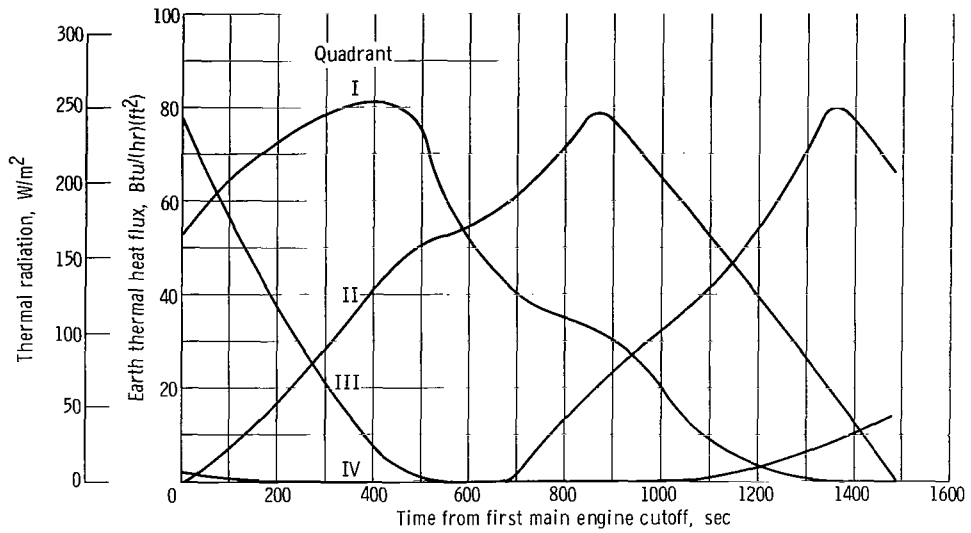
Figure 37. - AC-8 Centaur vehicle side wall environmental heat flux.
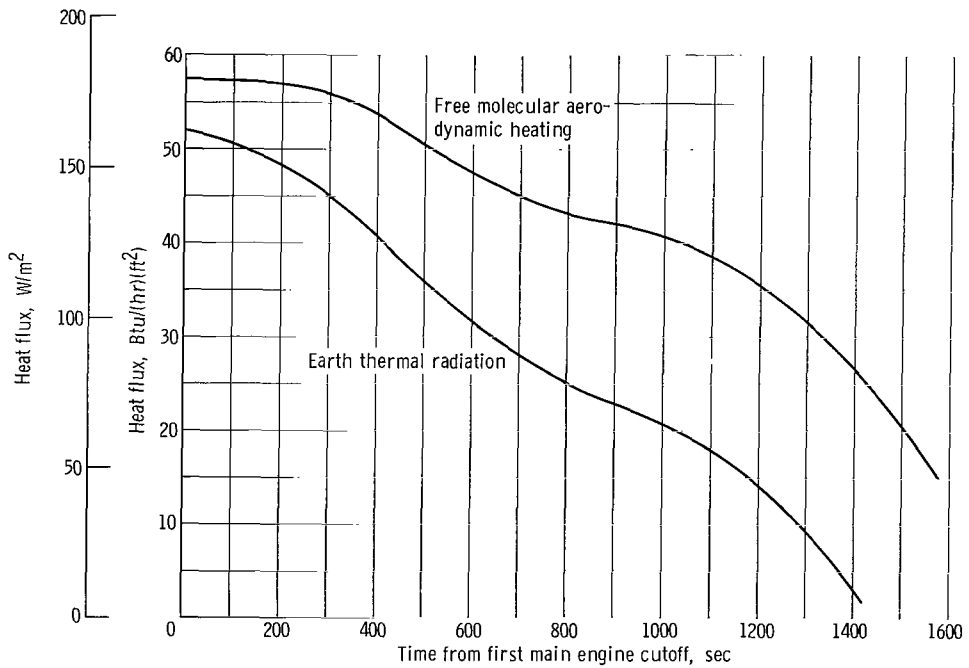
Figure 38. - AC-8 Centaur vehicle forward environmental heating.
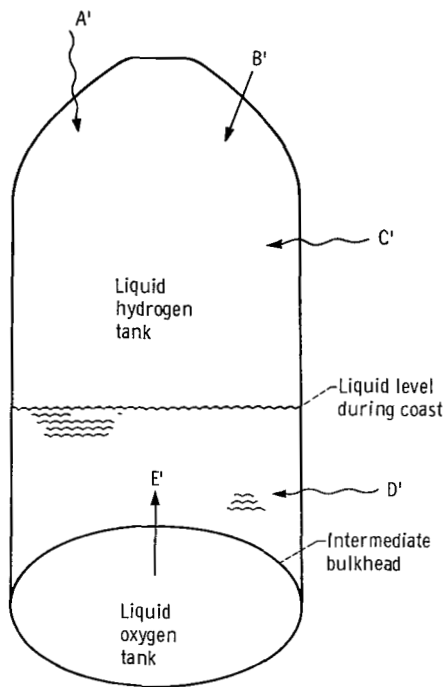
Input	Description	Heat rate	
		Btu/sec	W
A'	Net environmental heat rate to liquid hydrogen tank forward end unshadowed area	0.70	750
B'	Radiation and conduction from electronic components, payload adapter, and payload to hydrogen ullage	.28	290
C'	Net environmental heat rate to liquid hydrogen tank ullage side walls; area, 288 square feet (26.7 m^2)	.67	700
D'	Net environmental heat rate to liquid hydrogen; area, 209 square feet (19.4 m^2)	.48	500
E'	Conduction from intermediate bulkhead and boost pump feed lines to liquid hydrogen	.33	350

Figure 39. - Summary of heat rates to AC-8 Centaur hydrogen tank during coast period.

*"The aeronautical and space activities of the United States shall be
conducted so as to contribute . . . to the expansion of human knowl-
edge of phenomena in the atmosphere and space. The Administration
shall provide for the widest practicable and appropriate dissemination
of information concerning its activities and the results thereof."*

— NATIONAL AERONAUTICS AND SPACE ACT OF 1958

NASA SCIENTIFIC AND TECHNICAL PUBLICATIONS

TECHNICAL REPORTS: Scientific and
technical information considered important,
complete, and a lasting contribution to existing
knowledge.

TECHNICAL NOTES: Information less broad
in scope but nevertheless of importance as a
contribution to existing knowledge.

TECHNICAL MEMORANDUMS:
Information receiving limited distribution
because of preliminary data, security classifica-
tion, or other reasons.

CONTRACTOR REPORTS: Scientific and
technical information generated under a NASA
contract or grant and considered an important
contribution to existing knowledge.

TECHNICAL TRANSLATIONS: Information
published in a foreign language considered
to merit NASA distribution in English.

SPECIAL PUBLICATIONS: Information
derived from or of value to NASA activities.
Publications include conference proceedings,
monographs, data compilations, handbooks,
sourcebooks, and special bibliographies.

TECHNOLOGY UTILIZATION
PUBLICATIONS: Information on technology
used by NASA that may be of particular
interest in commercial and other non-aerospace
applications. Publications include Tech Briefs,
Technology Utilization Reports and Notes,
and Technology Surveys.

Details on the availability of these publications may be obtained from:

SCIENTIFIC AND TECHNICAL INFORMATION DIVISION

NATIONAL AERONAUTICS AND SPACE ADMINISTRATION
Washington, D.C. 20546